X-Rays and X-Ray Diffraction

3

3.1 Generation and Properties of X-Rays

X-rays are an electromagnetic radiation of short wavelength, and can be produced by the sudden deceleration of rapidly moving electrons at a target material. If an electron falls through a potential difference of V volt, it acquires an energy eV electron-volt (eV), where e is the charge on an electron. This energy may be expressed as quanta of X-rays of wavelength λ, where each quantum is given by

$$\lambda = hc/(eV) \tag{3.1}$$

h being the Planck constant and c the speed of light in vacuum. Substitution of numerical values into (3.1) leads to

$$\lambda = 12.4/V \tag{3.2}$$

where V is measured in kilovolt and λ is given in Angstrom units (Å). The wavelength range of X-rays is approximately 0.1–100 Å, but for the purposes of practical X-ray crystallography, the range used is restricted to 0.7–2.5 Å.

3.1.1 X-Rays and White Radiation

Except for synchrotron radiation, which is discussed in Sect. 3.1.6, a widely used source of X-rays in conventional crystallography laboratories is the sealed hot-cathode tube with a rotating anode, illustrated diagrammatically in Fig. 3.1. Electrons are emitted from a heated tungsten filament, the cathode, and accelerated by a high voltage, 40 kV or more, towards a water-cooled target anode, usually made of copper or molybdenum. A large proportion of the energy reaching the target is dissipated as heat on account of multiple collisions within the target material, but about 10% of it is converted usefully for X-ray crystallographic purposes. In order to dissipate the heat rapidly and efficiently, the water-cooled anode is rotated, as indicated in the diagram of Fig. 3.1.

M. Ladd and R. Palmer, *Structure Determination by X-ray Crystallography: Analysis by X-rays and Neutrons*, DOI 10.1007/978-1-4614-3954-7_3,
© Springer Science+Business Media New York 2013

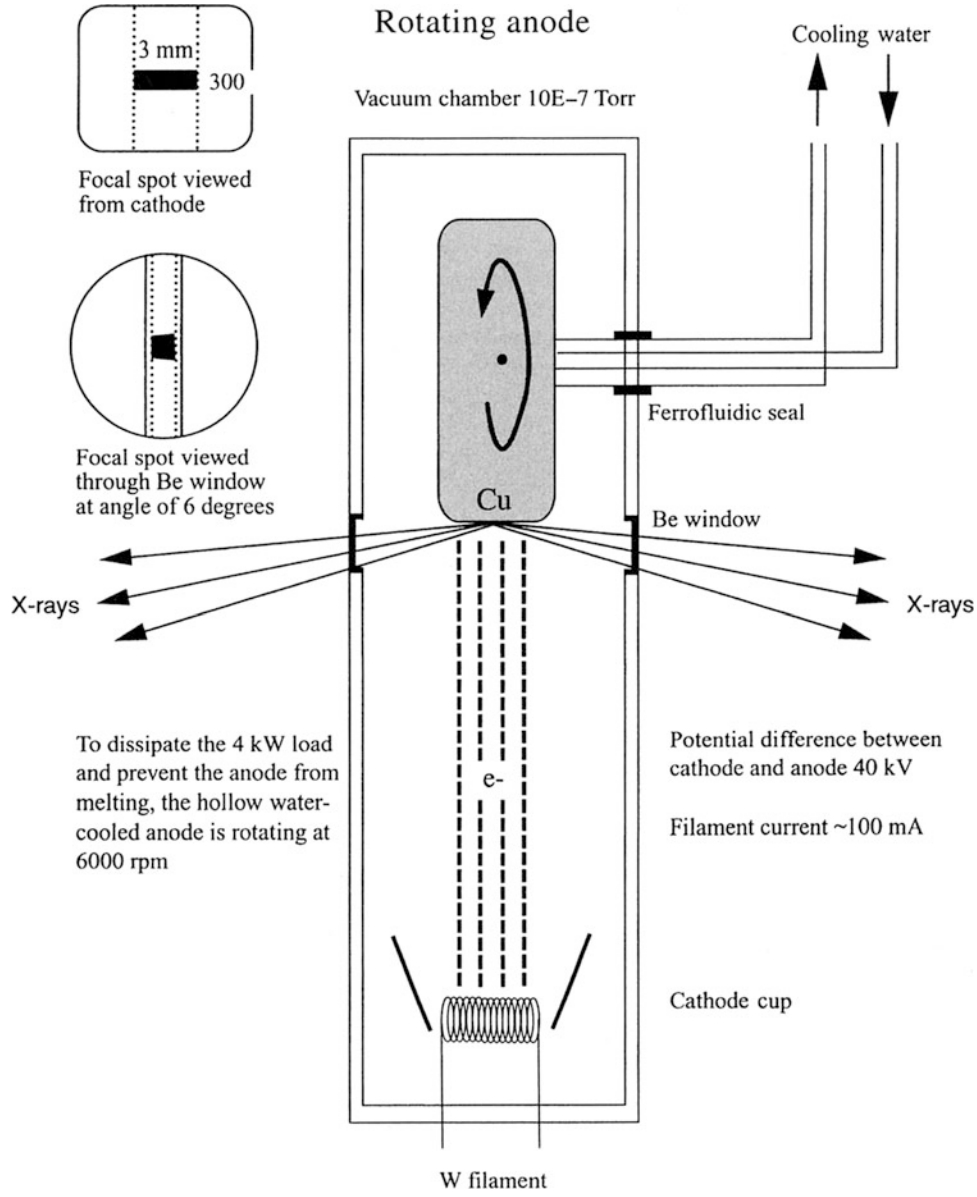

Fig. 3.1 Schematic diagram of a sealed crystallographic X-ray tube. The target anode is provided with a means of rotation, so as to aid the dissipation of heat generated by the electron impact on the target and to prolong the life of the target

As a consequence, a higher accelerating voltage can be applied to the tube, which results in a more powerful X-ray source. If the energy eV is not too high, there will be a continuous distribution of X-ray wavelengths, "white" radiation, or Bremsstrahlung (Ger. = braking radiation), as shown in Fig. 3.2. With an increase in the accelerating voltage V, the intensity of the radiation increases, and the maximum of the curve moves to shorter wavelengths.

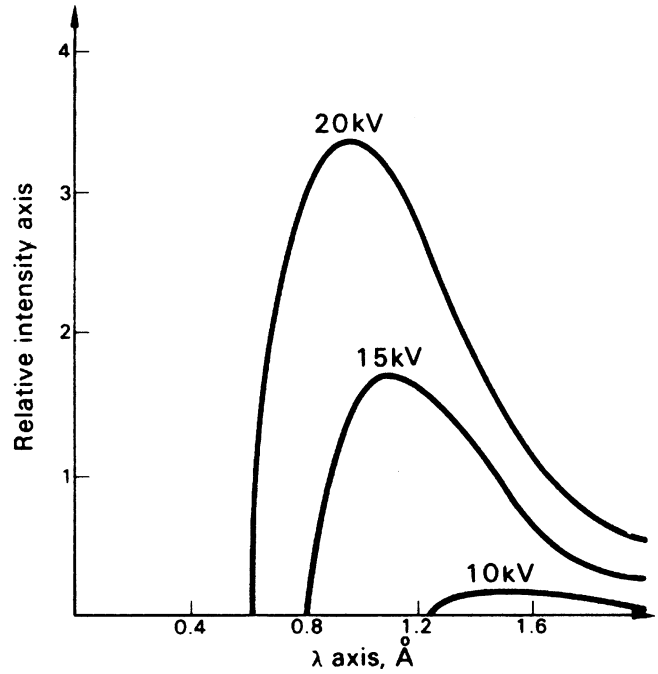

Fig. 3.2 Variation of intensity with wavelength for an X-ray tube, for three different operating voltages; as V increases, the maximum wavelength in the continuous spectrum moves to shorter wavelengths, in accordance with (3.2)

3.1.2 Characteristic Radiation

At a particular higher value of V, the impinging electrons excite inner electrons in the target atoms. Other electrons from higher energy levels then fall back to the inner levels, and their transitions are accompanied by the emission of X-radiation of high intensity, *characteristic* of the material of the target. The X-ray wavelength depends on the energies of the two levels involved, E_1 and E_2, such that

$$\lambda = hc/|E_2 - E_1| \tag{3.3}$$

Figure 3.3 illustrates the curve of radiation intensity against X-ray wavelength, when the accelerating voltage is sufficient to excite the K spectrum of the target metal. The K spectrum consists of the $K\alpha$ and $K\beta$ wavelengths, which are always produced together, and correspond to electrons falling back to the K level from the L and M levels respectively. Two slightly different L energy levels exist, so that the important $K\alpha$ spectrum consists of two components, $K\alpha_1$ and $K\alpha_2$, of closely similar wavelength. Similarly, $M \rightarrow K$ transitions give rise to $K\beta$ characteristic radiation. The wavelengths of the K radiations for a target material of copper are: $K\beta_1 = 1.39222$ Å, $K\beta_2 = 1.38109$ Å, $K\alpha_1 = 1.54056$ Å, and $K\alpha_2 = 1.54439$ Å. The mean value for $K\alpha$ is obtained by averaging the $K\alpha_1$ and $K\alpha_2$ wavelengths in their intensity ratio of 2:1, thus giving the average value of 1.54184 Å for $K\alpha$. The α_1, α_2 doublet is resolved when the angle of scatter is large, that is, at high values of the Bragg angle θ (q.v.).

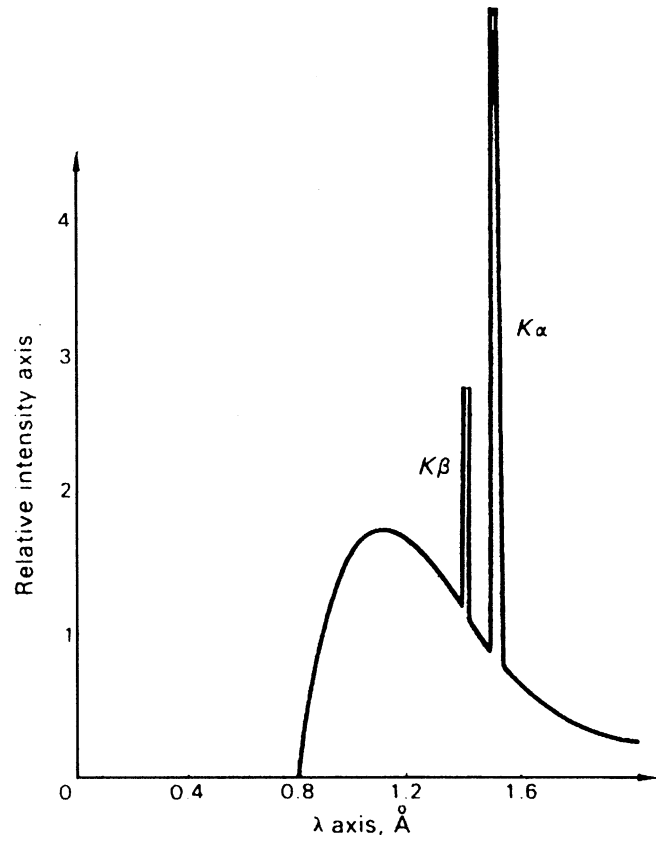

Fig. 3.3 Characteristic *K* spectrum from an X-ray tube superimposed upon the "white" radiation, or continuous spectrum

3.1.3 Absorption of X-Rays

All materials absorb X-rays, and the transmitted intensity is attenuated according to an exponential law:

$$I = I_0 \exp(-\mu t) \tag{3.4}$$

I_0 and I are, respectively, the incident and transmitted intensities, μ is the *linear absorption coefficient* of the material, and t is the path length for X-rays through the material. The absorption of X-rays increases with the atomic numbers of the elements in the absorbing material.

The variation of μ with wavelength is illustrated in Fig. 3.4, which refers to elemental nickel. The absorption coefficient μ of any material decreases approximately as $\lambda^{5/2}$, so that as λ falls, the energy of the radiation (hc/λ) becomes greater and more penetrating. With continuing decrease in wavelength, a position is reached where the energy of the radiation is sufficient to eject an electron from the L energy level of an atom of the material. At this point, known as the *absorption edge*, or *resonance level*, the value of μ is greatly enhanced. As the wavelength decreases further, the absorption coefficient continues to fall off as before. In the case of nickel, this particular L absorption edge occurs at a wavelength of 1.4886 Å.

Absorption edges are important in selecting the correct radiation for a particular application. For example, copper X-radiation would be unsuitable for materials containing a high percentage of iron. The K absorption edge for iron is 1.7433 Å, so that radiation of this wavelength would be strongly absorbed by the iron moiety and subsequently re-emitted as the characteristic K spectrum of iron. In such a case, molybdenum radiation, $\lambda(K\alpha) = 0.71073$ Å, would be a satisfactory alternative.

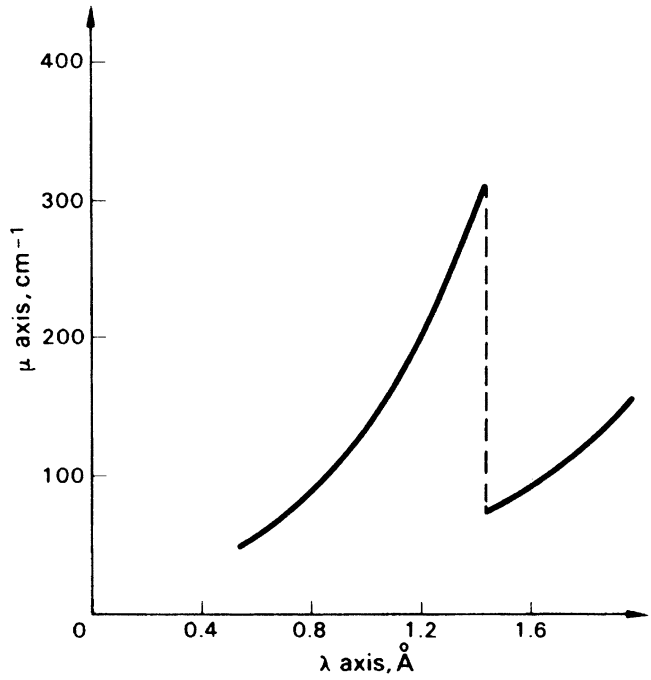

Fig. 3.4 Variation with wavelength of the linear absorption coefficient μ for nickel; the discontinuity at approximately 1.4886 Å corresponds with the L absorption edge of the element

If a material consists of a single elemental species, μ in (3.4) may be termed the atomic absorption coefficient [1] μ_a, given by

$$\mu_a = M_r \mu/(D_m L) \tag{3.5}$$

where M_r is the relative atomic mass, D_m the density of the material, and L the Avogadro constant. Of more general applicability is the *mass absorption coefficient* μ_m, given by $\mu_m = \mu/D_m$, so that $\mu_a = \mu_m(M_r/L)$. For a compound. we have

$$\mu = \sum_i \mu_{m,i} D_{m,i} \tag{3.6}$$

where $\mu_{m,i}$ is the mass absorption coefficient for the ith species of partial density $D_{m,i}$ in the compound; $D_{m,i}$ is calculated for the ith species as $D_{m,i}M_{m,i}/M_r$. For example, sodium chloride, NaCl, has a density of 2165 kg m^{-3}, and the relative atomic masses and mass absorption coefficients for Na and Cl are 22.98 and 3.01 m^2 kg^{-1}, and 35.45 m^2 kg^{-1} and 10.6 m^2 kg^{-1} for Na and Cl, respectively. Hence, the linear absorption coefficient for NaCl is given by

$$\mu = 2165[(3.01 \times 22.98/58.43) + (10.6 \times 35.45/58.43)] = 1.65 \times 10^4\ m^{-1}$$

and this parameter is needed in the correction of X-ray intensities, Sect. 4.1.3. The attenuation factor I/I_0, for a crystal of NaCl of thickness 0.1 mm in the path of the X-ray beam, is then $\exp(-1.65 \times 10^4 \times 0.1 \times 10^{-3})$, or 0.192.

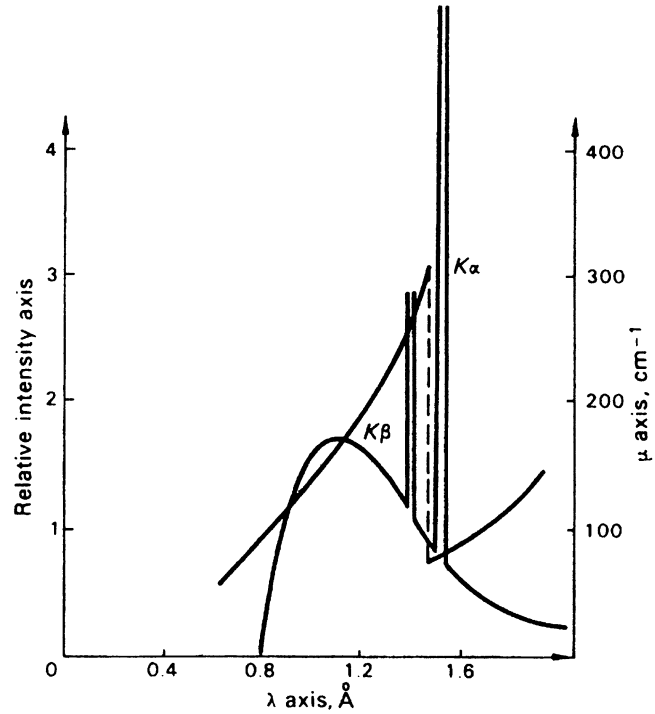

Fig. 3.5 Diagrammatic superposition of the curves of Figs. 3.3 and 3.4, for Cu $K\alpha$ X-radiation; the strongly preferential absorption of the $K\beta$ radiation results in an almost monochromatic $K\alpha$ radiation

3.1.4 Monochromatic Radiation

Usually X-ray structure analysis requires monochromatic radiation, but Figs. 3.2 and 3.3 show that X-ray sources contain a range of wavelengths. However, and in particular for radiation from a copper target, we note that the absorption edge for nickel (1.4886 Å) lies between the wavelengths for Cu $K\alpha$ and Cu $K\beta$ radiations. The effect of passing the X-rays from a copper target through a nickel foil of ca. 0.018 mm thickness is shown in Fig. 3.5, a superposition of Figs. 3.3 and 3.4. The $K\beta$ radiation is almost totally absorbed by the nickel, and the "white" radiation is decreased significantly in intensity. There is also a loss in intensity of the $K\alpha$ radiation, but the intense part of the beam behaves as a closely monochromatic, or *filtered*, radiation. Evidence for a residual presence of $K\beta$ and white radiation may be seen in Fig. 9.5 as weak reflections just below the strong reflections, that is, at lesser θ values; the very strong reflections also show spots from tungsten $L\alpha$ radiation at still lower θ values ($\lambda_{L\alpha} = 1.476$ Å). A similar degree of monochromatization can be obtained with molybdenum radiation if a filter of zirconium foil is used.

Crystals themselves can act as monochromators through application of the Bragg equation (q.v.); we consider this topic in Sect. 5.8.1ff.

3.1.5 Collimation

A collimator is used to define the angular limit of the X-ray beam. The simplest collimator is the pinhole type, a cylindrical device in which the beam is limited usually by two defining circular apertures together with a guard aperture. The collimation provided is satisfactory in many situations, and a divergence angle of approximately 0.02 rad is typical. Figure 3.6a illustrates an elegant apparatus for taking a back-reflection Laue photograph of a metal casting, showing also the type of collimator just described.

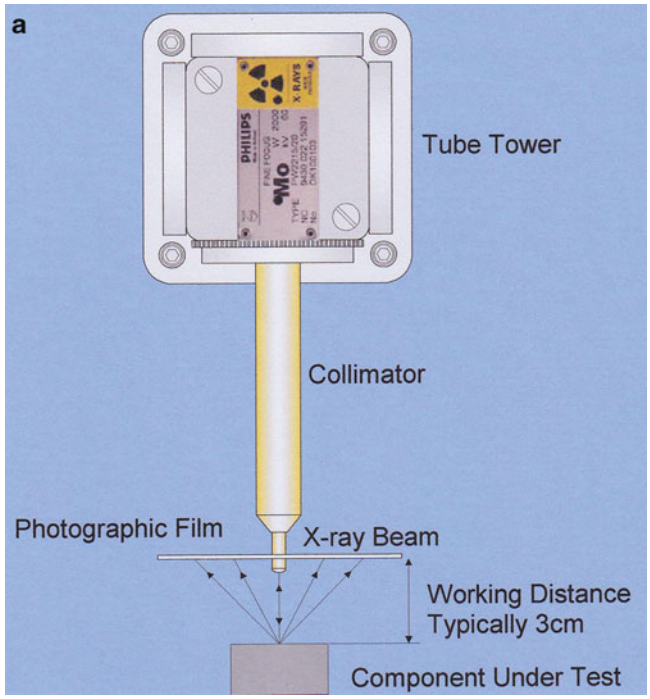

Fig. 3.6 Collimation of X-rays. (**a**) Collimator employed in a back-reflection Laue experiment (courtesy of Jackson Electronics Newark, UK)

(**b**) Cross-section of a multifiber polycapillary fiber collimator, with about 400 50 m diameter channels (Gibson D, Gibson W (2002) Adv X-ray Anal 45; reproduced by permission of ICDD)

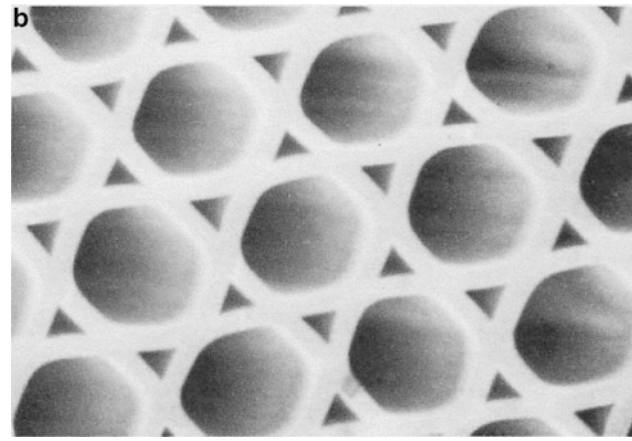

Improved collimators have been described [2] in which monochromatic X-rays, obtained by crystal reflection, are guided by multiple reflections within thin-walled borosilicate glass capillary tubes (Fig. 3.6b). It is necessary for the X-rays to be reflected from the tube walls at less than the critical angle θ_c:

$$\theta_c/\text{mrad} = 30/V$$

where the voltage V is measured in keV. The divergence at input could be 60–120 mrad, or 5–10°, and 2–4 mrad at output. The system allows a useful X-ray flux from Cu $K\alpha$ radiation to be produced that is four to five times stronger than that obtained by simple pinhole collimation, with comparable initial divergence, and the output beam produces uniform diffraction peaks while the higher energy Bremsstrahlung and background radiations are insignificant.

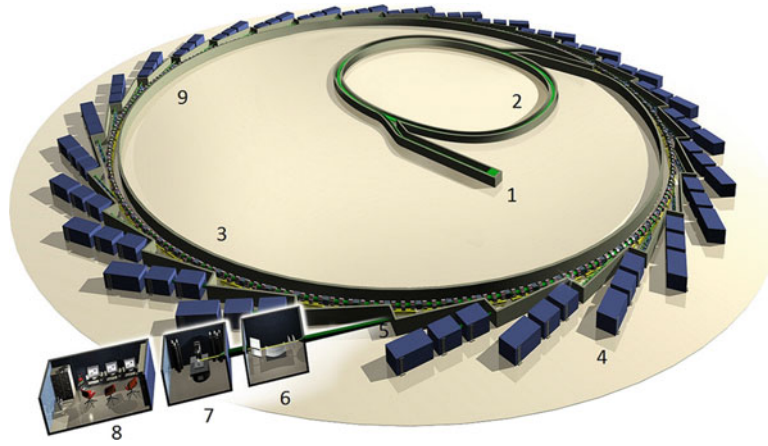

Fig. 3.7 Schematic illustration of the Diamond synchrotron facility at Harwell; the *numbered* sections are described in the text (reproduced by courtesy of the Diamond Light Source, Harwell Science and Innovation Campus)

3.1.6 Synchrotron Sources

A synchrotron is a large-scale particle accelerator designed primarily as a tool for fundamental studies in particle physics. However, it has many applications, and in X-ray crystallography it functions as a very powerful source of X-rays, with an intensity of several orders of magnitude greater than that of the sealed X-ray tube. It can generate brilliant beams of electromagnetic radiation from infra-red to X-ray wavelengths.

The Diamond Synchrotron Source

Figure 3.7 is a schematic diagram of the Diamond synchrotron that was opened at Harwell Science and Innovation Campus in 2007. It consists of several elements, as follow:

- In the *injection system* (1), an electron gun produces a series of pulses of electrons with an energy of approximately 90 keV. These electrons are then accelerated in the linear accelerator LINAC, which raises their energy to about 100 MeV.
- The 100 MeV electrons are further accelerated in the *booster synchrotron* (2). Thirty-six dipole bending magnets of field up to 0.8 T are used to curve the electron beam around the bends in the ring, and then they are ejected from the booster with energy of 3 GeV.
- The *storage ring* (3) contains 48 bending magnets that curve the electron beam between the straight sections. The total deflection is 360° and the length of the orbit is 561.6 m. The ring is under vacuum, and the 3 GeV electrons complete each circuit in 1.9×10^{-6} s, thus traveling at 98.6% of the speed of light.
- Each *beamline* (4) comprises three main sections: an optics hutch, an experimental hutch that houses experimental equipment, and a control hutch, and is designed for a specific experimental application.
- The *front end* (5) channels the synchrotron light into a beamline. It monitors the beam in passing through to the optics hutch.
- The *optics hutch* (6) contains mirrors and diffraction gratings or crystals, the purpose of which is to filter the beam so as to obtain the desired radiation wavelength, and also to focus it on to the sample under investigation.
- The *experimental hutch* (7) houses the technical equipment for carrying out the experiments and provides a number of different specialized X-ray detectors for the various kinds of experiments.

- The *control hutch* (8) provides the operators with a computer-controlled monitoring system for the experiment in progress.
- A *radiofrequency cavity* in the region of (9) contains an electromagnetic field that makes up for the energy that the electrons lose in the form of synchrotron radiation as they travel around the ring.

There is also *Diamond House*, which provides for Diamond staff accommodation, meeting, and conference rooms, and also access to the synchrotron facility itself.

The Diamond IO2 beamline, which is concerned with macromolecular X-ray crystallography, has a flux of about 1.5×10^{12} photon s^{-1} and, typically, an operating wavelength of 0.98 Å, giving a resolution of 1.09 Å. Beamlines IO3 and IO4 are similar to IO2, and beamlines IO4-1 and I24 are available for microfocus macromolecular crystallography. A fascinating video-description of a trip around the Diamond ring may be found at a web site [3].

Polarization of Synchrotron Radiation

An important difference between X-radiation from sealed tube or rotating anode sources and X-rays produced by a synchrotron is their physical state of polarization; see also Sect. 3.2.4. X-rays generated from conventional laboratory sources are totally non-polarized unless a crystal monochromator is employed. In contrast, synchrotron radiation is 100% linearly polarized in the plane of the electron beam orbit and elliptically polarized above and below the plane. In addition, the output radiation is pulsed, because the electrons do not form a uniform stream.

Figure 3.8a considers a three-dimensional X-ray wave at the origin, with components of oscillation vibrating in the y and z directions. The beam from a synchrotron is plane-polarized, with the component in the z direction being an order of magnitude less in intensity. X-ray beams from crystal monochromators, because they have undergone Bragg diffraction, are also polarized, but the extent is considerably less. The effect of this primary or beam polarization of synchrotron radiation on the intensity of the diffraction pattern must be taken into account during data processing. This is achieved through application of a *polarization factor* P that includes a source-dependent property, with components normal and parallel to the plane of polarization:

$$P = (I_{\parallel} - I_{\perp})/(I_{\parallel} + I_{\perp})$$

where $I_{\parallel}$ and $I_{\perp}$ are the intensities of the electrical fields of the X-ray beam along and normal to the axis of a rotation camera, respectively. The value of P is calibrated for each workstation at a synchrotron installation. For the Diamond station, P is approximately 0.8, whereas for a graphite monochromator, P is equal to 0.11.

A typical synchrotron radiation spectrum is shown in Fig. 3.8b and may be compared with that from the sealed tube. The photon intensity is given in units of photon per second for a horizontal angular aperture of 1 mrad (3.4 min of arc), with a 1 A beam current and a 0.1% spectral bandwidth, after performing vertical integration over the full angular divergence of the radiation above and below the orbital plane.

The flux attainable in practice depends upon the multiplying factors set by the values of the dependent parameters. A horizontal aperture of an experimental workstation may be less than 1 mrad for topography, typically 5–10 mrad for the majority of spectroscopy experiments, and up to 40 mrad for the high-aperture port used for time-resolved measurements. The flux available will change proportionally if this resolution is varied. The stored current and, hence the photo flux, gradually decline as electrons are lost by scattering from closed electron orbits. The beam lifetime, that is, the time of fall to approximately $1/e$ of the initial intensity, is approximately 8 h.

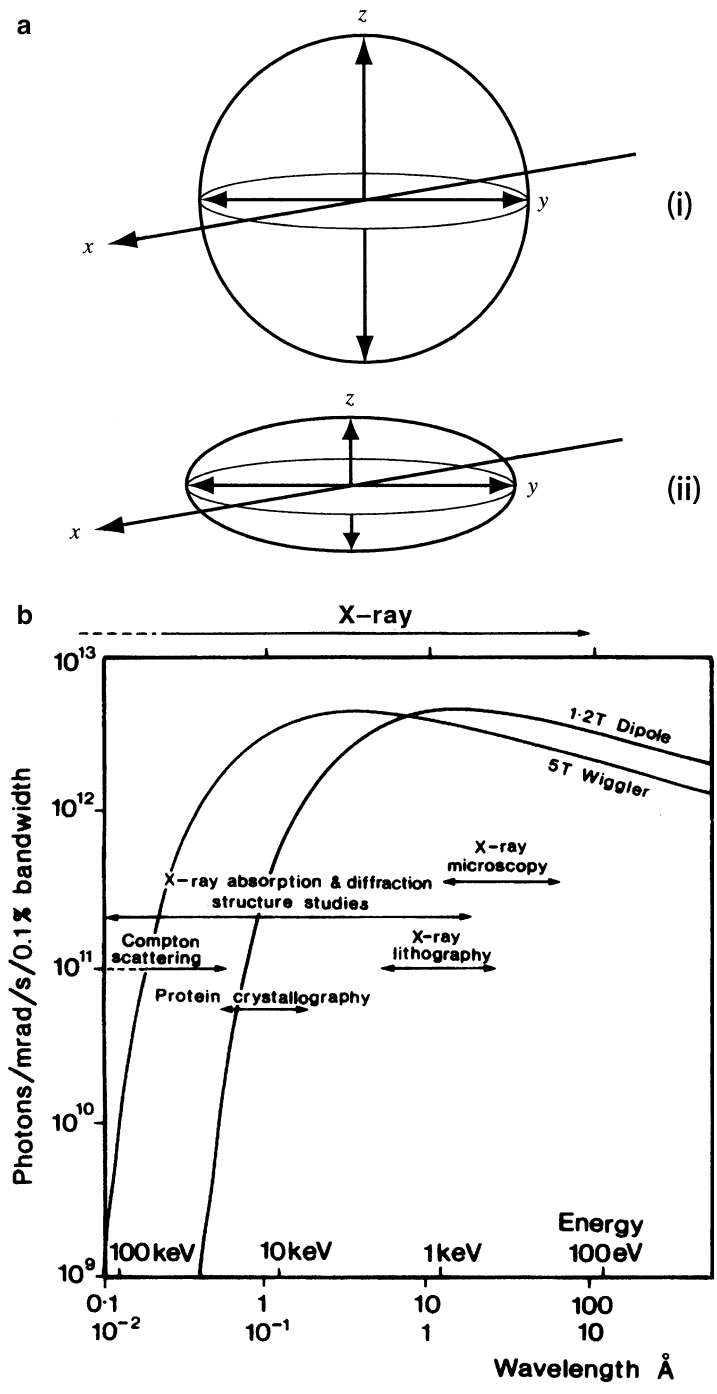

Fig. 3.8 (**a**) A three-dimensional wave traversing the origin, with oscillatory components vibrating along the x and y directions: (i) Conventional X-ray tube radiation, (ii) Synchrotron radiation (not to scale). The radiation from a synchrotron is plane-polarized, with the z component an order of magnitude less than that in the y direction. The spread of radiation in the vertical (z) direction is given as $\Delta = m_e c^2/E$, where E is the electron beam energy. (**b**) Spectral curves in the X-ray region from a normal bending magnet and a wiggler for a 2 GeV 1 A beam in the synchrotron radiation source, and the types of experiment used in the wavelength regions specified. The peak of the curve is approximately $1.4\lambda_c$, corresponding to the maximum output of energy per unit wavelength; λ_c is the critical wavelength for the synchrotron

Insertion Devices: Wigglers and Undulators

The output characteristics of the synchrotron can be modified by devices inserted into the straight sections between the magnets. An insertion device is an array of magnets which can be inserted into the straight sections of the storage ring and cause the electron beam to follow a wiggling or undulating

path, so as to produce more intense, tuneable light. Insertion devices come in two main types: wigglers and undulators.

A *wiggler* is an insertion device that consists of an array of dipolar magnets of alternating polarity which cause the electron beam to follow a wiggling path of oscillations perpendicular to its general direction. This causes the light to be produced in a wide cone, spanning a broad spectrum of X-rays. Wigglers are used in beamlines where the priority is for very high energy X-rays.

An *undulator*, which is more common at the Diamond installation, is an insertion device that produces a very bright light in a very narrow beam. By varying the separation of the magnet arrays, it is possible to tune the undulator and choose the energy that is generated. They can be used to produce very high energy X-rays over a continuous frequency range, which is essential for many experiments, particularly in protein crystallography.

The synchrotron source may be said to have revolutionized X-ray crystallography in certain applications. It has enabled a rapid collection of data to be achieved, and so is of great value in dealing with relatively unstable crystals, such as proteins, with poorly diffracting specimens or polymers, in time-resolved studies, or in solid-state reactions and other transformations, including enzyme-catalyzed processes, or in X-ray topographical studies of crystal defects.

Laser-Wakefield Acceleration

Relatively recent work on synchrotron sources has concentrated on a reduction in the physical size of the accelerator. If a high-powered, femtosecond (10^{-15} s) laser pulse is focused into a plasma, an electrostatic wake is produced which can be harnessed to accelerate electrons to GeV energies within centimeter distances. Electrons become separated from the positive ions, and a ponderomotive force, which is a non-linear force that a charged particle experiences in an inhomogeneous oscillating electromagnetic field, arising from the laser light pushes aside the plasma electrons so as to create a wake from the plasma. The associated electrostatic fields can produce an accelerating field of three to four orders of magnitude greater than in the conventional accelerator.

In one application of the procedure [4], a laser pulse of 37 fs is fired at a cell of hydrogen gas atoms, thus energizing the electrons and causing them to break free. The positive attraction of the nucleus acts to retain the electrons and the result is an oscillation about the nucleus that produces a plasma wave in the cell. This excitation is similar to the water-wave behind a motorboat; hence, the term wake-field (or wakefield). Other electrons "ride" this wave at relativistic speeds and so generate X-rays through their oscillatory changes.

An important feature in the process is the use of a miniature undulator. The combination of a 1.5 cm accelerator and a 30 cm magnetic undulator produced electron energies of 210 MeV. Further research aims at higher electron energies, so that laser-wakefield acceleration can generate X-rays in the useful wavelength range for diffraction experiments, and with facilities of centimeter size. This development has great potential for X-ray studies on proteins and viruses, where powerful X-ray sources are desirable, because of the low stability of some of these compounds.

3.2 X-Ray Scattering

Scattering occurs generally when electromagnetic radiation interacts with matter. Two everyday examples of scattering are the blue color of the sky and the haloes around distant car lights at night that arise from Rayleigh scattering, a highly wavelength-dependent elastic scattering of the light by gas molecules or dust particles in the air. The pattern seen when looking at a sodium street-lamp through a stretched handkerchief or an umbrella, which are approximately two-dimensional net structures, shows an aspect of diffraction similar to that which we shall be discussing with X-rays

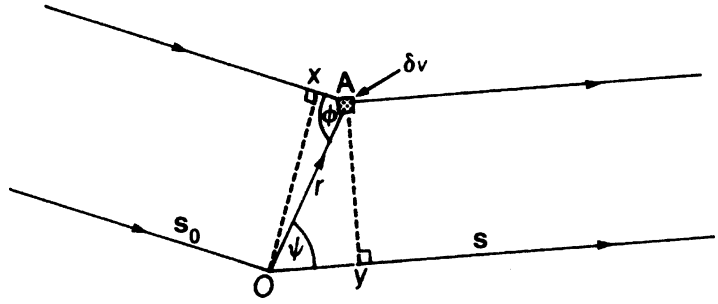

Fig. 3.9 Combined scattering at two centers O and A; $\mathbf{s}_0$ and $\mathbf{s}$ are unit vectors in the incident and scattered beams, respectively; δv is a small volume element at A.

and crystals, namely the interaction of radiation with a periodic distribution of matter. The X-ray scattering from a crystal is described in terms of the intensity of the scattering function and the angle of scatter.

3.2.1 Scattering by a Single Electron

If a plane monochromatic X-ray beam of wavelength λ is incident upon an electron at an origin O, then the amplitude $\Psi_{2\theta}$ of the scattered beam at a point P in the forward direction at unit distance from the origin is given by [5]

$$\Psi_{2\theta} = f_{2\theta}\Psi_0 \tag{3.7}$$

where Ψ_0 is the amplitude of the incident wave, 2θ is the scattering angle, and $f_{2\theta}$ is a constant of proportionality that we shall discuss more fully shortly.

3.2.2 Scattering by Two or More Electrons

Let a second electron be introduced at a point A, Fig. 3.9. We need now to determine the phase difference at any point P in the forward direction, where OP is much greater than OA, for the wavelets scattered by the two electrons. The path difference δ between the two wavelets scattered by O and A is $OY - AX$; thus the phase difference ϕ is $(2\pi/\lambda)\delta$, that is,

$$\phi = (2\pi/\lambda)(OY - AX) \tag{3.8}$$

If the distance OA is $|\mathbf{r}|$, then the incident and diffracted waves may be defined by the unit vectors $\mathbf{s}_0$ and $\mathbf{s}$, respectively, such that $AX = \mathbf{r}\cdot\mathbf{s}_0$ and $OY = \mathbf{r}\cdot\mathbf{s}$. Thus,

$$\phi = 2\pi(\mathbf{r}\cdot\mathbf{s} - \mathbf{r}\cdot\mathbf{s}_0)/\lambda = 2\pi\mathbf{r}\cdot(\mathbf{s}/\lambda - \mathbf{s}_0/\lambda) = 2\pi\mathbf{r}\cdot\mathbf{S} \tag{3.9}$$

From Fig. 3.10, it is clear that $\mathbf{S}$ is a vector normal to a plane through O that may be regarded conveniently as a *reflecting plane*; hence,

$$S = |\mathbf{s} - \mathbf{s}_0|/\lambda \tag{3.10}$$

so that the magnitude $|\mathbf{S}|$, or S, is equal to $2\sin\theta/\lambda$.

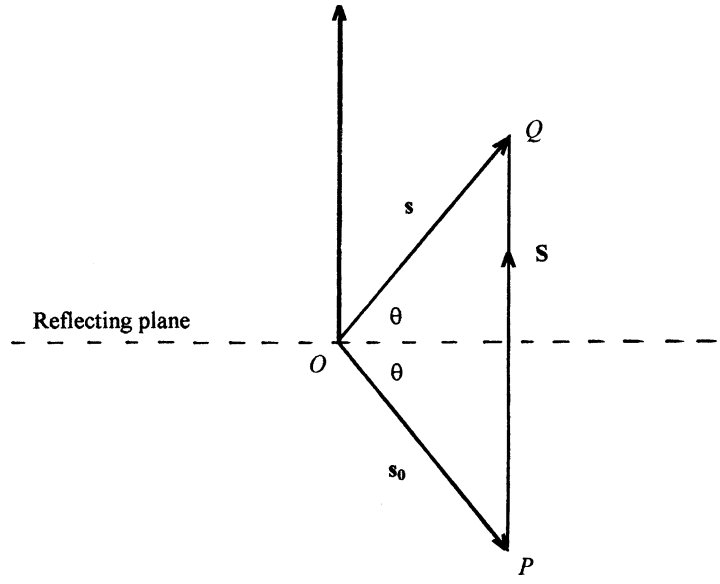

Fig. 3.10 Relationship of the scattering vector **S**, or $(\mathbf{s} - \mathbf{s}_0)/\lambda$, to the reflecting plane (*hkl*). The vector **S** is normal to the plane (*hkl*), and its magnitude $|\mathbf{S}|$, or S, is $2 \sin\theta/\lambda$

The amplitude of the wave scattered at P by the two electrons is thus

$$\Psi_{2\theta} = f_{2\theta} + f_{2\theta} \exp(\mathrm{i}2\pi\mathbf{r} \cdot \mathbf{S}) = f_{2\theta}[1 + \exp(\mathrm{i}2\pi\mathbf{r} \cdot \mathbf{S})] \tag{3.11}$$

The use of the exponential term to represent relative phase is explained below in Sect. 3.2.3 on the Argand Diagram. In the case that neither of the electrons of the previous example occupies the origin, so there is no zero relative phase involved, then the number 1 on the right-hand side of (3.11) would be replaced by another exponential term. In general, the result for n electrons is given by

$$\Psi_{2\theta,n} = f_{2\theta} \sum_{j=1}^{n} \exp(\mathrm{i}2\pi\mathbf{r}_j \cdot \mathbf{S}) \tag{3.12}$$

This equation assumes that the n scattering species have equal power, which would be true if they were all electrons, or identical atoms. In the event that the scattering species are unequal, then the function $f_{2\theta}$ would be unique to each species and included within the summation as $f_{2\theta,j}$. The scattering process itself introduces a phase shift with respect to the origin, but this applies equally to all atoms and may be ignored for our purposes.

3.2.3 Waves and Wave Sums

In (3.12), we considered the summation of waves of equal scattering power. In general, each scattering entity will be allocated its own scattering function and phase. Each wave then takes the form $f_j \exp(\mathrm{i}\phi_j)$, where $\phi_j = \mathbf{r}_j \cdot \mathbf{S}$. For convenience, we may drop the subscript θ (or 2θ) to f; unless we specifically want to emphasize its dependence on θ; we know that such dependence is always present. Using de Moivre's theorem, the exponential term may be expanded into cosine (real) and sine (imaginary) components: $\exp(\pm\mathrm{i}\phi) = \cos\phi \pm \mathrm{i}\sin\phi$, and a straightforward way of representing a wave is in the complex plane of an Argand diagram.

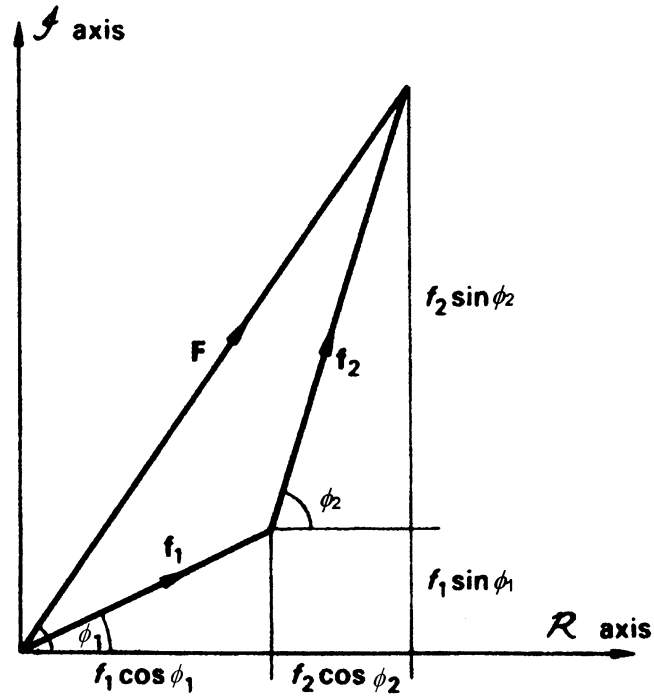

Fig. 3.11 Combination of the two waves $f_1 \exp(i\phi_1)$ and $f_2 \exp(i\phi_2)$, shown as vectors on an Argand diagram. The resultant is F, and its phase is expressed by the angle ϕ between F and the R (real) axis

Argand Diagram

In Fig. 3.11, we show the combination of two waves of scattering factors f_1 and f_2 on an Argand diagram to give a resultant F, which we shall later identify with the *structure factor*, Sect. 3.5.1:

$$\mathrm{F} = f_1 \exp(i\phi_1) + f_2 \exp(i\phi_2) \tag{3.13}$$

F is a scalar quantity but may be manipulated like a vector in the complex plane, having both a magnitude and direction; $\exp(i\phi)$ may be regarded as an operator that rotates f counterclockwise on an Argand diagram by the angle ϕ measured from the positive, real axis.

The foregoing analysis may be extended to n waves. The resultant sum F is, from (3.13),

$$\mathrm{F} = f_1 \exp(i\phi_1) + f_2 \exp(i\phi_2) + \cdots + f_j \exp(i\phi_j) + \cdots = \sum_{j=1}^{n} f_j \exp(i\phi_j) \tag{3.14}$$

The Argand diagram, Fig. 3.12, expresses (3.14) as a polygon of f-"vectors" for the combination of six waves, and the resultant F may be expressed as

$$\mathrm{F} = |\mathrm{F}| \exp(i\phi) \tag{3.15}$$

where the amplitude $|\mathrm{F}|$ is obtained from

$$|\mathrm{F}| = (\mathrm{F}\mathrm{F}^*)^{1/2} \tag{3.16}$$

F^* is the complex conjugate of F, that is, $|\mathrm{F}| \exp(-i\phi)$, Fig. 3.13. Resolving the resultant F of the six waves into its real and imaginary components, we have

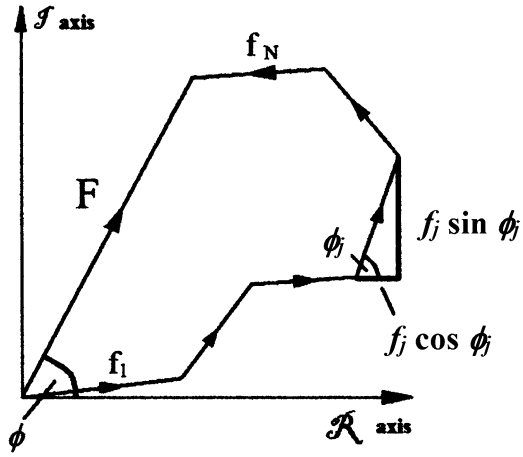

Fig. 3.12 Combination of six waves on an Argand diagram: $\mathrm{F} = \sum_{j=1}^{6} f_j \exp(\mathrm{i}\phi_j)$

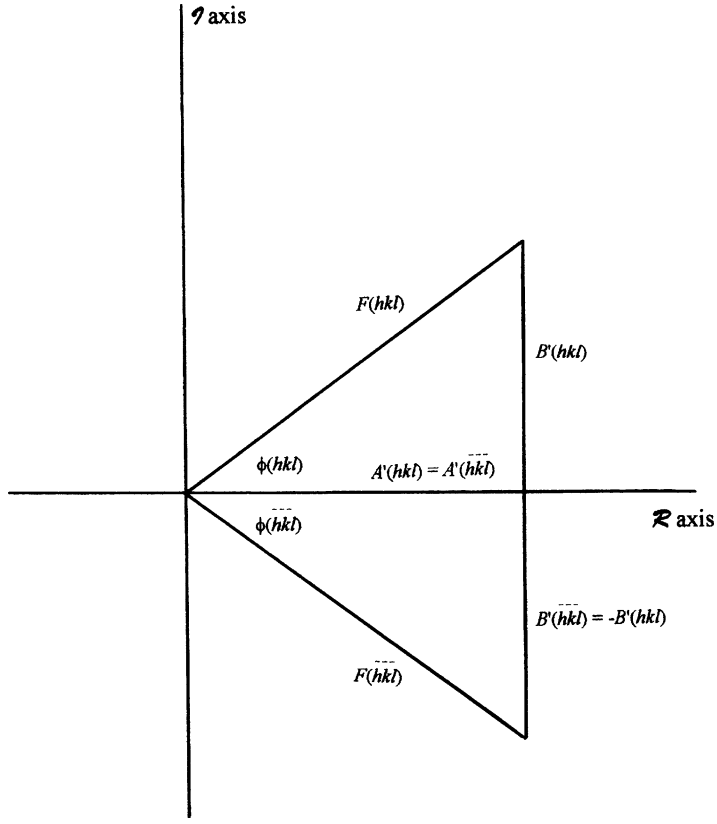

Fig. 3.13 The quantity F(*hkl*) for a reflection from an (*hkl*) family of planes and its components $A'(hkl)$ and $B'(hkl)$; $\phi(hkl)$ is the phase angle for F(*hkl*). The conjugate $\mathrm{F}^*(hkl)$, or $\mathrm{F}(\bar{h}\,\bar{k}\,\bar{l})$, has the same magnitude for A' and B', but the sign of B' is reversed; hence $\phi(hkl) = -\phi(\bar{h}\,\bar{k}\,\bar{l})$. In a centrosymmetric structure, F(*hkl*) lies along the real axis, so that $\mathrm{F}(hkl) = A'(hkl)$, or $F(hkl)$, and its phase is either 0 or π. Then, since $A'(hkl) = |\mathrm{F}(hkl)| \cos \phi$, it is common to speak of the *sign* of F(*hkl*), that is, $\pm F(hkl)$, in a centrosymmetric structure

$$|\mathrm{F}| = (A'^2 + B'^2)^{1/2} \tag{3.17}$$

where

$$A' = \sum_{j=1}^{n} f_j \cos \phi_j \tag{3.18}$$

and

$$B' = \sum_{j=1}^{n} f_j \sin \phi_j \tag{3.19}$$

The phase ϕ of the resultant F is given by

$$\phi = \tan^{-1}(B'/A') \tag{3.20}$$

Graphical Representation of Wave Sums

When waves of equal frequency, those in which we are interested, combine, the resultant can be determined through (3.17–3.20). If two waves are in exact register—path difference, $n\lambda$—the resultant amplitude is simply the sum of the individual amplitudes. If the waves are exactly out of phase—path difference, $(n + 1)\lambda/2$—the resultant is the difference between the amplitudes. All cases between these extremes are possible, depending on the values of the amplitudes |F| and phase angles ϕ. In Fig. 3.14, we represent the combination of two waves, one of amplitude 100 (f_1) and phase 0°, and the other of amplitude 50 (f_2) and phase 240°, with respect to the origin. From the foregoing, the amplitude of the resultant becomes

$$|\mathrm{F}| = [(f_1 \cos \phi_1 + f_2 \cos \phi_2)^2 + (f_1 \sin \phi_1 + f_2 \sin \phi_2)^2]^{1/2} \tag{3.21}$$

and the phase of the resultant is

$$\phi = \tan^{-1} [(f_1 \sin \phi_1 + f_2 \sin \phi_2)/(f_1 \cos \phi_1 + f_2 \cos \phi_2)] \tag{3.22}$$

Importance of Correct Phases

As shown in the legend to Fig. 3.14, the resultant amplitude |F| is 86.6 and its phase ϕ is 330°. From the figure we can see the importance of the correct phase of a wave (reflection). The peaks (atomic positions) in this figure occur at 330° ± 2π (±360°). If, on one hand, we decrease f_2 to 25, the resultant amplitude is 90.1, because the sine term subtracts a smaller amount, and the phase is 346°, a small change in position. If on the other hand, we decrease the phase by half, leaving f_2 unchanged, then the resultant amplitude is again 86.6, but the phase (atomic position) is now at +30°, a very different situation; see Problem 7.11.

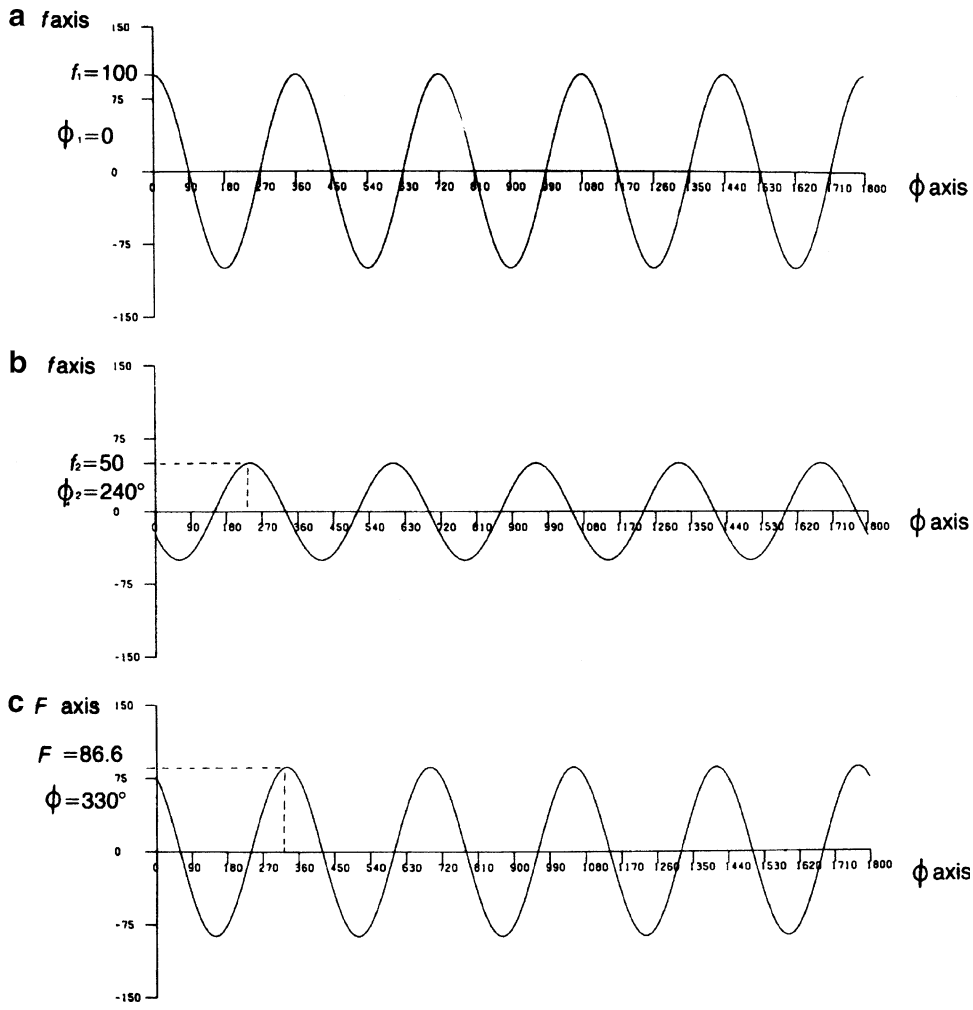

Fig. 3.14 Combination of two waves of amplitudes 100 (f_1) and 50 (f_2) with phases 0° (ϕ_1) and 240° (ϕ_2), respectively. The resultant wave has an amplitude |F| and a phase ϕ. (**a**) First wave. (**b**) Second wave. (**c**) Resultant wave F, given by $= [(100 + 50 \cos 240)^2 + (50 \sin 240)^2]^{1/2} = 86.6$; $\phi = \tan^{-1}[(50 \sin 240)/(100 + 50 \cos 240)] = -30°$ (330°)

3.2.4 Coherent and Incoherent Scattering

Coherent (Thomson) Scattering: Polarization

In coherent scattering, the incident and scattered waves have the same wavelength, and there is a definite phase relationship between the incident and scattered radiations. When X-rays fall upon an electron, the alternating electric-field vector imparts an alternating acceleration to the electron. Classical electromagnetic wave theory shows that an accelerated charged particle emits radiation, through a process of absorption and re-emission, the emitted radiation traveling in all directions for a given angle of scatter. A theoretical treatment of Thomson scattering [5] shows that the intensity $I_{2\theta}$ of the scattered radiation of incident intensity I_0, defined as power per unit solid angle, is

$$I_{2\theta} = \frac{1}{2}[e^2/(4\pi\varepsilon_0 c^2 m_e)]^2(1 + \cos^2 2\theta)I_0 \tag{3.23}$$

where e is the charge on an electron, ε_0 is the permittivity of a vacuum, c is the speed of light in a vacuum, and m_e is the mass of the electron. The factor $1/m_e$ shows how electrons are the only effective scattering species for X-rays: even the lightest species, hydrogen, although it has the same magnitude of charge, is ca. 1,840 times heavier than the electron. This result shows also that neutrons are excluded from the category of X-ray scattering species because they are uncharged particles. The term $\frac{1}{2}(1 + \cos^2 2\theta)$ is a geometrical factor known as the *polarization factor* p for X-ray scattering, which we shall encounter further in ensuing chapters.

$$p = \frac{1}{2}(1 + \cos^2 2\theta) \tag{3.24}$$

Incoherent (Compton) Scattering
With incoherent scattering, the wavelength of the scattered radiation is longer than that of the incident radiation, which implies a loss of energy in the scattering process, owing to elastic collisions of electrons with photons. An analysis [5] shows that in Compton scattering, the wavelength change $\delta\lambda$ is given by

$$\delta\lambda = [h/(m_e c)](1 - \cos 2\theta) \tag{3.25}$$

or, by inserting the fundamental constants in appropriate units,

$$\delta\lambda\,(\text{A}) = 0.0243(1 - \cos 2\theta) \tag{3.26}$$

Thomson scattering illustrates the particle property of the electron, whereas Compton scattering shows its wave nature.

3.2.5 Scattering by an Atom

In an atom, electrons are bound in levels of distinct energies, and in the scattering of X-rays by an atom both coherent and incoherent scattering are involved. A full analysis of the scattering process requires a wave-mechanical treatment, involving both modes of scattering, from which we obtain the electron density function ρ, where $\rho = \Psi\Psi^*$ and Ψ^* is conjugate to Ψ; if we assume a real nature for the electron density function then $\rho = |\Psi|^2$, and the expression may be interpreted such that $\Psi^2\,\mathrm{d}\tau$, or $\rho\,\mathrm{d}\tau$, represents the probability of finding the electron in a volume element $\mathrm{d}\tau$. We shall use the Thomson formula only because incoherent scattering contributes to the background radiation and is but a small fraction of the total intensity in the case of crystalline materials.

Consider a plane of atoms in a crystal. We demonstrate in the ensuing sections that all atoms on this plane scatter in phase with one another and with the atoms in parallel planes, for a given scattering vector **S**. Thus, we need to consider how the electrons in any one atom combine in order to obtain the total scattering amplitude for the atom.

Let $\rho(\mathbf{r})\,\mathrm{d}\tau$ be the probability that an electron in the chosen atom lies in a small volume element $\mathrm{d}\tau$ distant r from the origin, the center of the atom, where r is the magnitude of the vector **r**, as shown in Fig. 3.15. If $f(\mathbf{S})$ represents the scattering power of the atom in the direction **S**, then we have from the foregoing:

$$f(\mathbf{S}) = \int \rho(\mathbf{r}) \exp(\mathrm{i}2\pi\mathbf{r}\cdot\mathbf{S})\,\mathrm{d}\tau \tag{3.27}$$

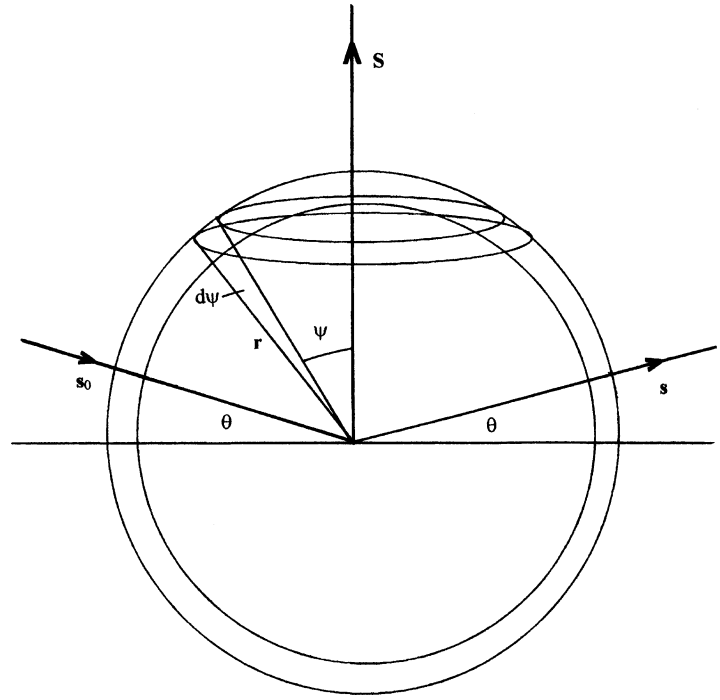

Fig. 3.15 Scattering by a single atom. A section of a sphere of radius r, showing an annular ring of thickness dr at an angle Ψ to the scattering vector **S**. The volume of the annular ring is $[\pi(r + \mathrm{d}r)^2 - \pi r^2]r \sin \Psi \, \mathrm{d}\Psi = 2\pi r^2 \sin \Psi \, \mathrm{d}\Psi \, \mathrm{d}r$ (neglecting second order terms in dr)

Let **S** make an angle Ψ with the direction of r. Then

$$2\pi \mathbf{r} \cdot \mathbf{S} = (4\pi/\lambda) \sin\theta \, r \cos \Psi = mr \cos \Psi$$

where $m = 4\pi(\sin\theta)/\lambda$. Since spherical symmetry has been assumed, the volume element dτ is a spherical annulus of radius r and thickness dr on **S** as axis, so that $\mathrm{d}\tau = 2\pi r^2 \, \mathrm{d}\Psi \, \mathrm{d}r$.

Let $mr \cos \Psi = x$, so that $\mathrm{d}x = -mr \sin \Psi \, \mathrm{d}\Psi$. Now (3.27) may be expressed as

$$f(\mathbf{S}) = 2\pi \int_0^\infty r^2 \rho(r)/mr \, \mathrm{d}r \int_{mr}^{-mr} -\exp(\mathrm{i}x) \, \mathrm{d}x = 4\pi \int_0^\infty r^2 \rho(r)(\sin mr)/mr \, \mathrm{d}r \tag{3.28}$$

Since $m = (4\pi \sin\theta)/\lambda$, (3.28) may be recast as a function of $|\mathbf{S}|$:

$$f(\mathbf{S}) = 4\pi \int_0^\infty r^2 \rho(r)(\sin 2\pi rS)/(2\pi rS) \, \mathrm{d}r \tag{3.29}$$

where S is $2 \sin\theta/\lambda$.

The atomic scattering factor may be defined as *the ratio of the amplitude of coherent scattering from an atom to that scattering by a single electron at the center of the atom*. It follows from (3.29) that, for scattering in the forward direction, when $(\sin 2\pi rS)/(2\pi rS) = 1$, the expression $\int_0^\infty r^2 \rho(r) \, \mathrm{d}r$ becomes the total electron density for the atom. Hence, we may write

$$f(\mathbf{S})_{S=0} = Z \tag{3.30}$$

where Z is the total number of electrons in the atom, or atomic number; $S = 0$ is equivalent to $\sin\theta = 0$ in terms of the θ-angle.

As an example calculation, we consider the contribution of a $1s$ electron to $f(\mathbf{S})$. We equate $\rho(r)$ to $|\Psi_{1s}|^2$ and use Slater's analytical wavefunctions. The Slater one-electron $1s$ wavefunction Ψ_{1s} may be written as $(1/\sqrt{\pi})c_1^{3/2}\exp(-c_1/r)$; c_1 is $(Z - \sigma)/a_0$, where σ is Slater's quantum mechanical screening constant [6] and a_0 is the Bohr radius for hydrogen. With lithium, for example, $\sigma_{1s} = 0.30$ and, remembering that $\rho \propto \Psi^2$, we have from (3.29),

$$f_{1s}(\mathbf{S}) = 2c_1^3/(\pi S)\int_0^\infty r\exp(-c_1 r)\,\sin(2\pi S r)\,\mathrm{d}r$$

From a table of standard integrals, or by use of the Γ function (see Web Appendix WA7),

$$\int_0^\infty x\exp(-ax)\,\sin(bx)\,\mathrm{d}x = 2ab/(a^2+b^2)^2$$

so that

$$f_{1s}(\mathbf{S}) = c_1^4/(c_1^2+\pi^2S^2)^2 \tag{3.31}$$

In lithium, for example, there are two contributions from (3.31) and one contribution from a similar expression for the $2s$ electron (see also Problem 3.3). They are added to obtain the value of f at a given value of $\mathbf{S}$. Atomic scattering factor data are readily available, quoted normally as functions of $\sin\theta/\lambda$. Such data refer to systems of electrons at rest: at a finite temperature, the effective scattering from an atom is less than the value at rest, and we shall discuss this situation later in this chapter. A satisfactory calculation of rest atomic scattering factors is afforded by the equation

$$f(s) = \sum_{j=1}^{4} a_j\exp(-b_j s^2) + c_j \tag{3.32}$$

where s is $\sin\theta/\lambda$, and the nine constants required by the equation have been recorded for all atomic and some ionic species [7].

3.3 Scattering by Regular Arrays of Atoms

The interaction of X-rays with a crystal is a complex process, often described as a diffraction phenomenon although, strictly speaking, it is a combined scattering and interference effect. Two treatments, those of von Laue and Bragg, describe the process, and we shall consider them in that order.

3.3.1 Laue Equations

Figure 3.16 represents a regular, one-dimensional array of atoms of spacing b, imagined in three-dimensional space. Parallel X-rays are incident at an angle ϕ_2 and scattered at an angle Ψ_2 to the direction of $\mathbf{b}$. The path difference for rays scattered by neighboring centers is represented by

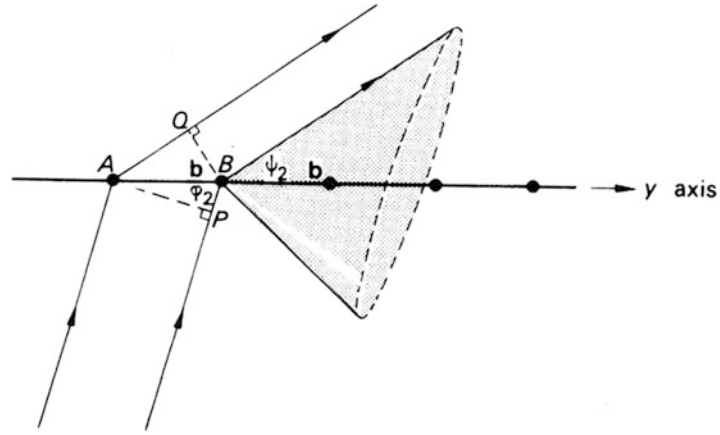

Fig. 3.16 Diffraction from a row of scattering centers, of spacing b along the y axis. The Laue equation $b(\cos \Psi_2 - \cos \phi_2) = k\lambda$, or $\mathbf{b} \cdot \mathbf{S} = k$, is satisfied by any generator of the cone

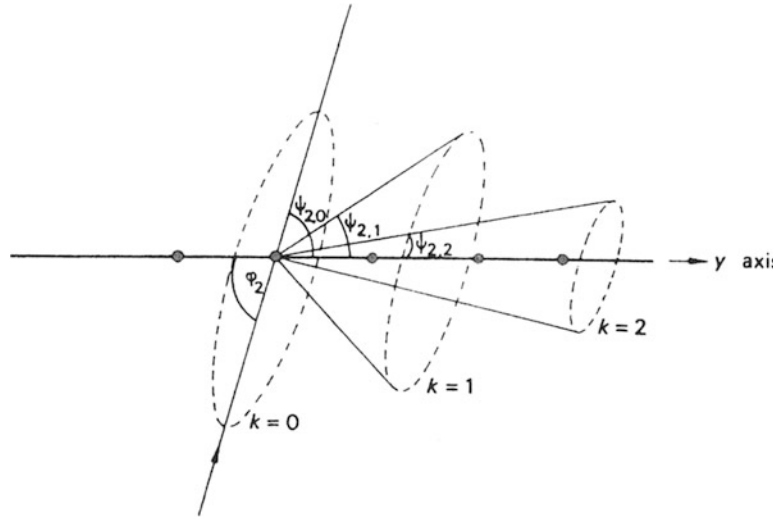

Fig. 3.17 Several orders of diffraction can arise from a row of scattering centers, for a given value of ϕ_2, corresponding to integral values for k

$AQ - BP$, or $b(\cos \Psi_2 - \cos \phi_2)$; this difference must be equal to an integral number of wavelengths for reinforcement to occur, so that

$$b(\cos \Psi_2 - \cos \phi_2) = k\lambda = \mathbf{b} \cdot \mathbf{s} - \mathbf{b} \cdot \mathbf{s}_0 \tag{3.33}$$

where $\mathbf{s}$ and $\mathbf{s}_0$ have meanings as before. This equation may be written alternatively, using (3.10), as

$$\mathbf{b} \cdot (\mathbf{s} - \mathbf{s}_0)/\lambda = \mathbf{b} \cdot \mathbf{S} = k \tag{3.34}$$

The generators of a cone of semivertical angle Ψ_2, coaxial with the row in Fig. 3.16, satisfy (3.33). For a given value of ϕ_2, there will be a series of cones corresponding to the orders of k ($k = 0, 1, 2, \ldots$), as shown in Fig. 3.17.

The discussion is extended readily to a net a, b, so giving rise to a second condition

$$\mathbf{a} \cdot (\mathbf{s} - \mathbf{s}_0)/\lambda = \mathbf{a} \cdot \mathbf{S} = h \tag{3.35}$$

A second cone now intersects the first cone generally in two lines, but for the special case that both (3.34) and (3.35) hold simultaneously, the two lines coincide and the atoms of the net scatter in phase, with the incident and diffracted beams lying in the plane of the net.

Generalizing the argument to three dimensions, we obtain the complete Laue equations:

$$\begin{aligned} \mathbf{a} \cdot \mathbf{S} &= h \\ \mathbf{b} \cdot \mathbf{S} &= k \\ \mathbf{c} \cdot \mathbf{S} &= l \end{aligned} \tag{3.36}$$

Any of the three possible pairs of equations define scattering from the corresponding net, but for the particular case that all three equations apply simultaneously, the three-dimensional array scatters in phase and produces the *hkl* spectrum.

Referring to Fig. 1.12 *mutatis mutandis*, we can rewrite (3.36) as

$$\begin{aligned} \mathbf{a} \cdot \mathbf{S} &= 2a \sin\theta/\lambda \cos\alpha = h \\ \mathbf{b} \cdot \mathbf{S} &= 2b \sin\theta/\lambda \cos\beta = k \\ \mathbf{c} \cdot \mathbf{S} &= 2c \sin\theta/\lambda \cos\gamma = l \end{aligned} \tag{3.37}$$

where h, k, and l are integers. The direction cosines cos α, cos β, and cos γ of the vector **S**, normal to the reflecting plane, with respect to the directions of **a**, **b**, and **c** are, therefore, proportional to a/h, b/k, and c/l, respectively. Successive planes (hkl) in the crystal intersect the x, y, and z axes at a/h, b/k, and c/l, respectively, so that they are parallel to the reflecting plane (hkl). Thus, (3.37) show that a scattered beam may be considered as derived from the incident beam by "reflection" from the (hkl) family of planes. Furthermore, if $d(hkl)$ is the interplanar spacing, then from Sect. 1.2.2,

$$d(hkl) = a/h \cos\alpha = b/k \cos\beta = l/c \cos\gamma \tag{3.38}$$

and (3.37) shows that

$$2d(hkl) \sin\theta = \lambda \tag{3.39}$$

a relation deduced by Bragg, originally in the form $2d(hkl) \sin \theta = n\lambda$.

3.3.2 Bragg Equation

The deduction of the Bragg equation, sometimes thought to be ad hoc, was occasioned by the observation that if a crystal in a position that produced a scattered X-ray beam was rotated through an angle φ to another scattering position, then the scattered beam had been rotated through 2φ, as in the reflection of light from a plane mirror.

In Fig. 3.18, two planes from a family of planes (hkl) are shown, together with the incident and reflected rays. The part of the incident beam that is not reflected at a given level passes on to be

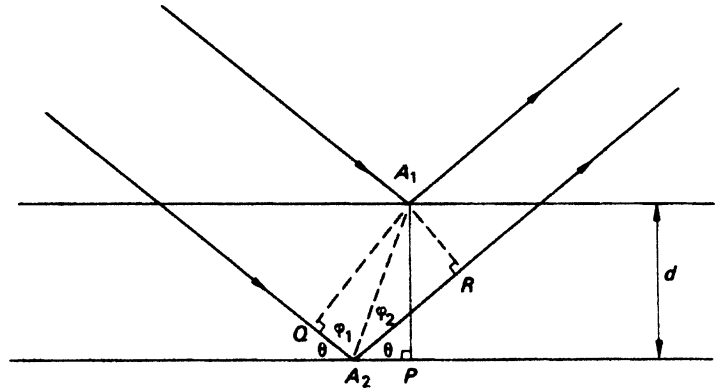

Fig. 3.18 Geometry of X-ray reflection. The path difference between the two typical rays reflected from successive planes is ($QA_2 + A_2R$). When this difference is equal to an integral number of wavelengths λ, a reflection is obtained, according to the Bragg equation

reflected from a deeper level in the crystal. Furthermore, all rays reflected from a given level remain in phase after reflection, because there is no path difference between them.

The path difference δ between the two reflected rays shown is given by

$$\begin{aligned}\delta &= QA_2 + A_2R = A_1A_2\cos\phi_2 = A_1A_2(\cos\phi_1 + \cos\phi_2)\\ &= 2A_1A_2\cos[(\phi_1 - \phi_2)/2]\cos[(\phi_1 + \phi_2)/2]\end{aligned} \tag{3.40}$$

which, by simple manipulation, becomes

$$\delta = 2d\sin\theta \tag{3.41}$$

Since δ is independent of ϕ_1 and ϕ_2, (3.41) applies to all rays in the bundle reflected from the adjacent planes. By the usual rules that apply to the combination of waves, the reflected rays will interfere with one another, the interference being at least partially destructive unless the path difference δ is equal to an integral number of wavelengths. Hence, we obtain the Bragg equation, as originally formulated:

$$2d\sin\theta = n\lambda \tag{3.42}$$

where n is an integer. The mirror-reflection analogy breaks down in practice because this equation must be satisfied for a reflection to occur, but the treatment is, nevertheless, a very useful geometrical way of looking at the X-ray diffraction process.

In (3.42), n is the *order* of the Bragg reflection. From Sect. 2.4, we recall that $d(hkl)/n = d(nh, nk, nl)$, with h, k, and l taking common factors as necessary. Thus, n is included in the definition of $d(hkl)$, and the Bragg equation now written as

$$2d(hkl)\ \sin\theta(hkl) = \lambda \tag{3.43}$$

Each reflection from a crystal must now be considered, effectively, as first-order from the (hkl) family of planes, specified uniquely by their Miller indices. To illustrate this argument further, Table 3.1 lists data for planes parallel to (120) in a cube of side 5 Å.

The Bragg and von Laue treatments are equivalent, and we shall use them as the occasion demands. It has been convenient for this discussion, although not necessary, to consider

Table 3.1 Nomenclature for interplanar spacings

Original Bragg notation			Current usage	
hkl	Order	*d* (Å)	*hkl*	*d* (Å)
120	1	2.236	120	2.236
	2	2.236	240	1.118
	3	2.236	360	0.745
	4	2.236	480	0.559

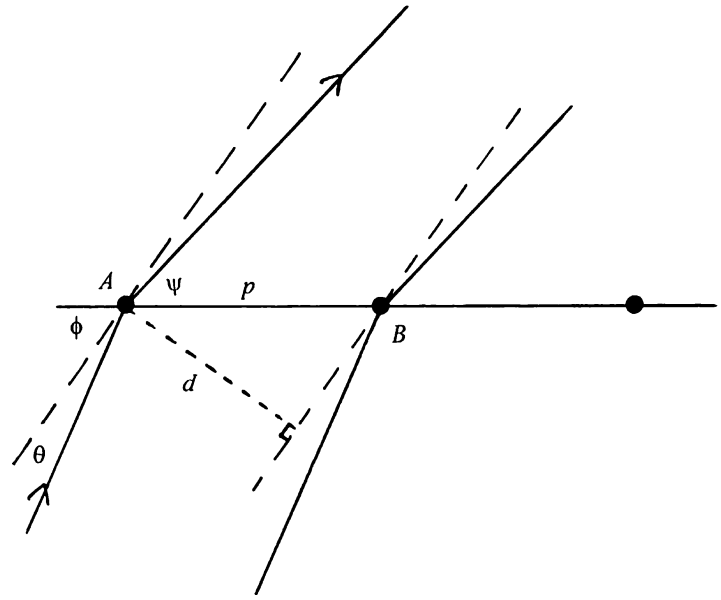

Fig. 3.19 Equivalence of the Laue and Bragg treatments of X-ray diffraction

that the scattering material is concentrated at lattice points, or on lattice planes. In general, electron density is a continuous function, albeit with a lattice-like distribution in the crystal.

3.3.3 Equivalence of the Laue and Bragg Equations

A way of demonstrating the equivalence between the Laue and Bragg treatments is illustrated by Fig. 3.19. Let p be the spacing between adjacent scattering points A and B in any row of a three-dimensional lattice. An X-ray beam makes the incident angle ϕ with the row of points, and Ψ is the angle between the diffracted ray and the same row. A "reflecting" plane must be in such a position as to make an angle θ with both rays; the dashed line in the figure is the trace of such a plane. Following Sect. 3.3.1, we write

$$p(\cos \Psi - \cos \phi) = n\lambda \tag{3.44}$$

where m is an integer. Expanding (3.44), we obtain $-2p \sin((\Psi + \varphi)/2) \sin((\Psi - \varphi)/2) = n\lambda$.

It follows from the diagram that $\phi - \theta = \Psi + \theta$ so that $(\phi/2) = (\Psi/2) + \theta$, whereupon $p \sin((\Psi + \phi)/2) = p \sin(\Psi + \theta) = d$ and $((\Psi - \phi)/2) = (\Psi/2) - ((\Psi/2) + \theta) = -\theta$. Hence,

$$2d \sin\theta = n\lambda \tag{3.45}$$

which is the Bragg equation (3.42) derived above.

3.3.4 Further Analysis of the Path Difference

In (3.12) we expressed the resultant wave from n scattering centers, there thought of as electrons. Now, we can consider them as atoms each specified in scattering power by $f(\mathbf{S})$.

The contribution to a wave scattered by the Ath atom in a unit cell is given by $f_A(\mathbf{S})\exp(\mathrm{i}2\pi\mathbf{r}_A \cdot \mathbf{S})$, where the exponential term is the phase of the contribution from the Ath atom. Now the distance r from the origin to atom A is expressed through

$$\mathbf{r}_A = x_A\mathbf{a} + y_A\mathbf{b} + z_A\mathbf{c} \tag{3.46}$$

where x_A, y_A, and z_A are the fractional coordinates of atom A, as before. Since $|\mathbf{S}| = 2\sin\theta(hkl)/\lambda$, which from (3.43) is $1/d(hkl)$, or $d^*(hkl)$ (taking κ as 1), $\mathbf{S}$ is the reciprocal lattice vector $\mathbf{d}^*(hkl)$. Applying (2.15) we have

$$\mathbf{r}_A \cdot \mathbf{S} = (x_A\mathbf{a} + y_A\mathbf{b} + z_A\mathbf{c}) \cdot (h\mathbf{a}^* + k\mathbf{b}^* + l\mathbf{c}^*) = hx_A + ky_A + lz_A \tag{3.47}$$

since $\mathbf{a} \cdot \mathbf{a}^* = 1$, and $\mathbf{a} \cdot \mathbf{b}^* = 0$, and similarly for b and c.

Thus, from (3.12), the phase angle ϕ_A for an atomic species A and its phase contribution are now given by $2\pi\mathbf{r}_A \cdot \mathbf{S}$, or

$$\phi_A = 2\pi(hx_A + ky_A + lz_A) \tag{3.48}$$

and the phase contribution is, therefore, $\exp[\mathrm{i}2\pi(hx_A + ky_A + lz_A)]$.

3.4 Reciprocal Lattice: Analytical Treatment

We considered a geometrical derivation of the reciprocal lattice in Sect. 2.4, as we believe that treatment forms a straightforward introduction to it. Here, we shall discuss the reciprocal lattice in greater detail.

In considering the stereographic projection, we showed that the morphology of a crystal could be represented by a bundle of lines, drawn from a point, normal to the faces of the crystal. This description, although angle-true, lacks linear definition. The representation may be extended by giving each normal a length that is inversely proportional to the corresponding interplanar spacing in real space, and applying it to *all* possible lattice planes, so forming a reciprocal lattice.

Let a Bravais (real-space) lattice be represented by the unit cell vectors $\mathbf{a}$, $\mathbf{b}$, $\mathbf{c}$. The reciprocal lattice unit cell is defined by the vectors $\mathbf{a}^*$, $\mathbf{b}^*$, $\mathbf{c}^*$, such that $\mathbf{a}^*$ is perpendicular to $\mathbf{b}$ and $\mathbf{c}$, and so on. Then,

$$\mathbf{a}^* \cdot \mathbf{b} = \mathbf{a}^* \cdot \mathbf{c} = \mathbf{b}^* \cdot \mathbf{a} = \mathbf{b}^* \cdot \mathbf{c} = \mathbf{c}^* \cdot \mathbf{a} = \mathbf{c}^* \cdot \mathbf{b} = 0 \tag{3.49}$$

The magnitudes of the reciprocal unit cell vectors are defined by

$$\mathbf{a}^* \cdot \mathbf{a} = \mathbf{b}^* \cdot \mathbf{b} = \mathbf{c}^* \cdot \mathbf{c} = \kappa \tag{3.50}$$

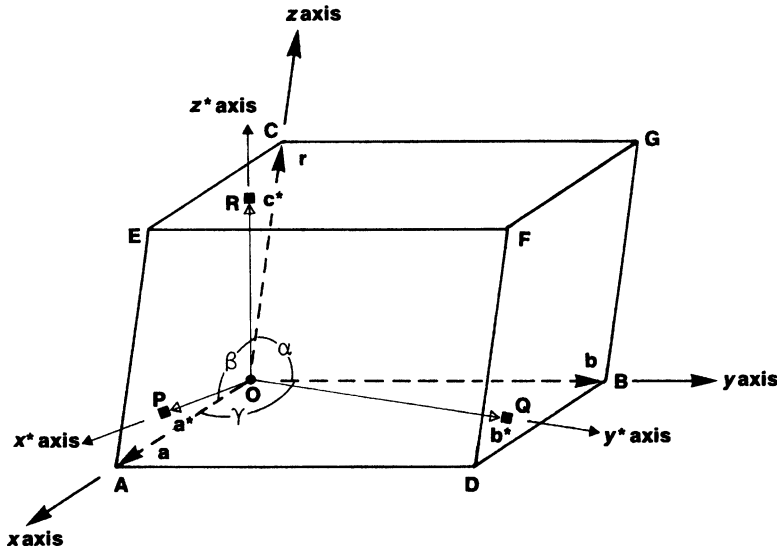

Fig. 3.20 Triclinic unit cell, showing its vectors **a**, **b**, and **c**, and the corresponding reciprocal unit-cell vectors, $\mathbf{a}^*$, $\mathbf{b}^*$, and $\mathbf{c}^*$

where κ is a constant, normally equal to unity in theoretical discussions, and to an X-ray wavelength in practical applications where the size of the reciprocal lattice is important.

In Fig. 3.20, the $z^*(c^*)$ axis is normal to the plane a, b. Since $\mathbf{c} \cdot \mathbf{c}^* = cc^* \cos \angle COR$, that is, taking $\kappa = 1$ in this discussion,

$$c^* = |\mathbf{c}^*| = 1/(c \cos \angle COR) \tag{3.51}$$

the magnitude of $\mathbf{c}^*$ in reciprocal space is inversely proportional to the c-spacing in real, or Bravais, space; similar deductions can be made for both $\mathbf{a}^*$ and $\mathbf{b}^*$. Since $\mathbf{c}^*$ is normal to both **b** and **c**, it lies in the direction of their vector product:

$$\mathbf{c}^* = \eta(\mathbf{a} \times \mathbf{b}) \tag{3.52}$$

where η is a constant. Let V be the unit cell volume in real space. Then,

$$V = \mathbf{c} \cdot (\mathbf{a} \times \mathbf{b}) \tag{3.53}$$

Now $\mathbf{a} \times \mathbf{b}$ is a *vector* of magnitude $ab \sin \gamma$, the area of $OADB$, directed normal to the plane of a, b and forming a right-handed set of directions with **a** and **b**. Then,

$$\mathbf{c} \cdot \mathbf{c}^* = \eta \mathbf{c} \cdot (\mathbf{a} \times \mathbf{b}) = \eta V = 1 \tag{3.54}$$

Hence,

$$c^* = |\mathbf{c}^*| = (ab \sin \gamma)/V \tag{3.55}$$

with values for a^* and b^* obtained by cyclic permutation.

The angle γ^* between $\mathbf{a}^*$ and $\mathbf{b}^*$ can be obtained by the equations of spherical trigonometry (see Web Appendices WA2 and WA3). From the discussion therein, we derive

$$\cos\gamma^* = (\cos\alpha\cos\beta - \cos\gamma)/\sin\alpha\sin\beta \tag{3.56}$$

with corresponding expressions for α^* and β^* obtained by cyclic permutation. Simplified expressions obtain for (3.51)–(3.56) when the crystal symmetry is higher than triclinic.

3.4.1 Reciprocal Lattice Properties

In the Web Appendix WA6, we derive a number of useful properties of the reciprocal lattice, and we summarize the results here.

Unit-Cell Volumes in Real and Reciprocal Space
The volume of the unit cell may be evaluated as follows. From (3.53), and expressing **a**, **b,** and **c** in terms of a set of orthogonal unit vectors, we derive the equation for a unit-cell volume V_c in terms of its six constants, as shown in Web Appendix WA6; thus

$$V_c = abc(1 - \cos^2\alpha - \cos^2\beta - \cos^2\gamma + 2\cos\alpha\cos\beta\cos\gamma)^{1/2} \tag{3.57}$$

In the same Appendix, we show also that

$$V_c V^* = \kappa \tag{3.58}$$

where V^* is the volume of the reciprocal unit cell and κ has the meaning as before.

Interplanar Spacings
From (2.16), the general equation for $d^*(hkl)$ is obtained in terms of the reciprocal unit cell constants from

$$\begin{aligned}|\mathbf{d}^*(hkl)|^2 &= (h\mathbf{a}^* + k\mathbf{b}^* + l\mathbf{c}^*)\cdot(h\mathbf{a}^* + k\mathbf{b}^* + l\mathbf{c}^*)\\ &= h^2a^{*2} + k^2b^{*2} + l^2c^{*2} + 2klb^*c^*\cos\alpha^* + 2lhc^*a^*\cos\beta^* + 2hka^*b^*\cos\gamma^*\end{aligned} \tag{3.59}$$

and so

$$\sin^2\theta(hkl) = \lambda^2/[4d^2(hkl)] = \lambda^2 d^{*2}(hkl)/4 \tag{3.60}$$

Simplifications of (3.59) arise in the presence of symmetry higher than triclinic and have been detailed adequately in Table 2.4.

Angle Between Planes
Given any two planes $h_1k_1l_1$ and $h_2k_2l_2$, the angle between them can be found as the supplement of the angle between the two normals, $d^*(h_1k_1l_1)$ and $d^*(h_2k_2l_2)$; this angle is the *interfacial angle* of the stereographic projection, Sect. 1.3.

In general, the angle ϕ between the forward directions of two vectors **p** and **q** is given through

$$\cos\phi = (\mathbf{p}\cdot\mathbf{q})/pq \tag{3.61}$$

Table 3.2 Limiting conditions for centered unit cells

Unit-cell-type	Limiting conditions	Associated translations	Structure factor multiplier G
P	None	None	1
A	hkl: $k + l = 2n$	$b/2 + c/2$	2
B	hkl: $l + h = 2n$	$c/2 + a/2$	2
C	hkl: $h + k = 2n$	$a/2 + b/2$	2
I	hkl: $h + k + l = 2n$	$a/2 + b/2 + c/2$	2
F	hkl: $h + k = 2n$ hkl: $k + l = 2n$ hkl: $(l + h = 2n)$[a]	$a/2 + b/2$ $b/2 + c/2$ $c/2 + a/2$	4
R_{hex}[b]	hkl: $-h + k + l = 3n_{obv}$	$a/3 + 2b/3 + 2c/3$ $2a/3 + b/3 + c/3$	3
	or hkl: $h - k + l = 3n_{rev}$	$a/3 + 2b/3 + c/3$ $2a/3 + b/3 + 2c/3$	3

[a]This condition is not independent of the other two
[b]See Sect. 2.2.3 and Table 2.3

Applying (2.16) for the two planes $h_1k_1l_1$ and $h_2k_2l_2$, we find

$$\cos\phi = [h_1h_2a^{*2} + k_1k_2b^{*2} + l_1l_2c^{*2} + (k_1l_2 + k_2l_1)b^*c^*\cos\alpha^* + (l_1h_2 + l_2h_1)c^*a^*\cos\beta^* + (h_1k_2 + h_2k_1)a^*b^*\cos\gamma^*]/[d^*(h_1k_1l_1)d^*(h_2k_2l_2)] \tag{3.62}$$

Reciprocity of F and I Unit Cells

We show in the Web Appendix WA6 how an F unit cell reciprocates into an I unit cell (and conversely), where the I unit cell is defined by the vectors $2\mathbf{a}_F^*$, $2\mathbf{b}_F^*$, and $2\mathbf{c}_F^*$. If, as is customary in practice, we define the reciprocal of an I unit cell by vectors $\mathbf{a}_F^*$, $\mathbf{b}_F^*$, and $\mathbf{c}_F^*$, then only those reciprocal lattice points for which each of $h + k$, $k + l$ (and $l + h$) is an even integer belong to the reciprocal of the I unit cell. In other words, Bragg reflections from an F unit cell have indices of the same parity; see also Sect. 3.7.1 and Table 3.2.

3.4.2 Reciprocal Lattice and Reflection Condition: Ewald Sphere

A section of a reciprocal lattice is shown in Fig. 3.21a: the vectors $\mathbf{s}_0/\lambda$ and $\mathbf{s}/\lambda$ lie in the incident and scattered X-ray beams respectively; a crystal is situated at the point C. The vector QP, which is also the direction of $\mathbf{S}$, must be normal to an (hkl) plane and have the magnitude $2\sin\theta/\lambda$. When the conditions for diffraction are satisfied, according to (3.43), $S = |\mathbf{d}^*(hkl)|$. A sphere of radius $1/\lambda$ is described on C as center, and passing through Q, the origin of the reciprocal lattice. If another reciprocal lattice point, such as P, lies on the sphere, then a diffracted beam arises and the vector CP is the direction of this beam; the incident beam vector is along CQ. The sphere is known as the *sphere of reflection*, or *Ewald sphere* [8], and will be required in subsequent chapters. We note that although we always refer to the "Ewald" sphere, the first suggestion for this device came from Bernal [9].

Figure 3.21b is an alternative way of looking at the Ewald sphere construction, in this case taking the radius of the sphere as unity, so that reciprocal space has the units of length^{-1}. The conclusions from the construction are, of course, the same, as we can see: from the figure $AQ = 2$ and $\angle APQ = 90°$, so that $QP = AQ\ \sin\theta(hkl)$, or $2\sin\theta(hkl)$. From (3.43), $2\sin\theta\ (hkl) = \lambda/d(hkl)$, and from Sect. 2.4, we may identify the point P with the reciprocal lattice point hkl. Hence, $QP = d^*(hkl)$. Since $\kappa = \lambda$ in this construction, $d^*(hkl) = 2\sin\theta(hkl)$. Thus, the reflection from the (hkl)

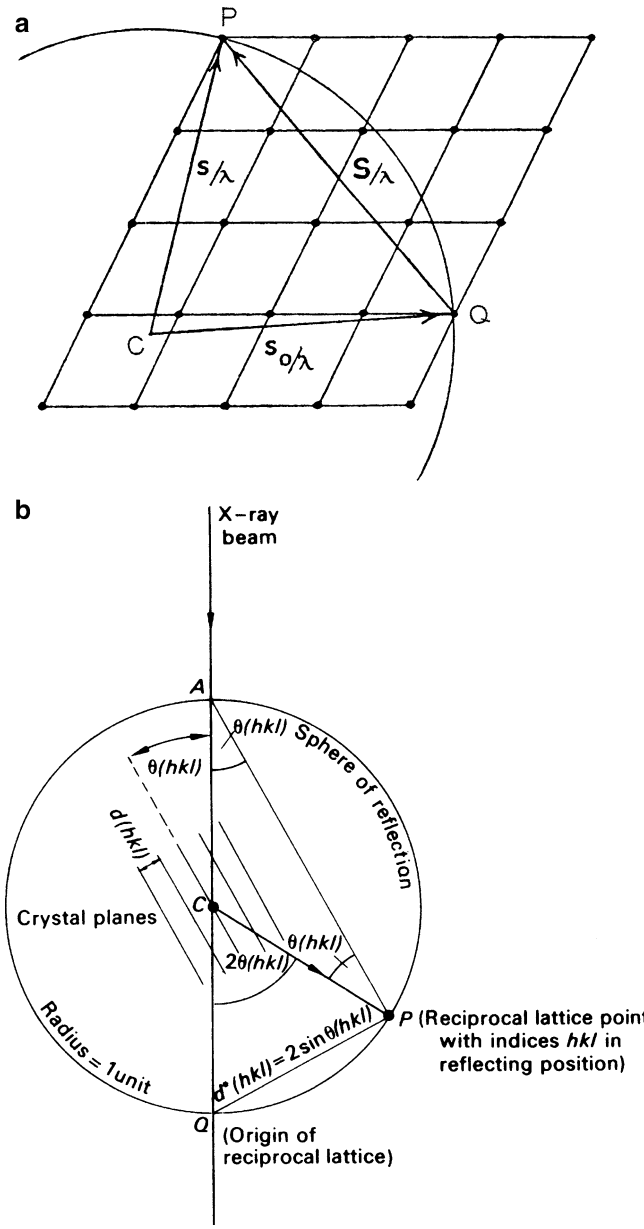

Fig. 3.21 (**a**) Sphere of reflection, radius $1/\lambda$, with the crystal at C, the center. The origin of the reciprocal lattice is at Q. When a reciprocal lattice point, such as P, lies on the Ewald sphere, a reflection arises along the direction CP. (**b**) Alternative, equivalent picture, but with the sphere of radius 1 (dimensionless), showing the position of crystal planes. By geometry, QP is parallel to the normal $d^*(hkl)$ to the crystal planes and is now $2\sin\theta(hkl)$

plane occurs when the *hkl* reciprocal lattice point lies on the sphere of reflection, and the direction of reflection is, again, that of CP.

3.5 Scattering by a Crystal Structure

In Sect. 2.2ff, we discussed the geometrical properties of the lattices on which crystal structures are based and showed how the arrays of atoms or molecules may be arranged according to space-group symmetry. We need next to consider the diffraction of X-rays by a crystal. We refer the process of scattering to a conventional unit cell and determine the resultant effect of all atoms in the unit cell,

which leads directly to the equation for the structure factor, F. The scattering of X-rays by a crystal comprises two parts: a geometrical part that depends on the symmetry of the arrangement of its components, and a structural part that depends upon both the nature of the atoms or molecules comprising those entities and their relative positions in the unit cell.

3.5.1 Structure Factor Equation

We need to express the equation that has been deduced for F in a manner that includes the coordinates of the atoms in the unit cell. It follows from (3.46)–(3.48) that the phase for the *j*th atom, with respect to the origin, can be represented by $2\pi(hx_j + ky_j + lz_j)$. Hence, we use this expression in (3.14) to give the structure factor equation for the *hkl* reflection:

$$\mathrm{F}(hkl) = \sum_{j=1}^{n} f_{j,\theta} \exp[\mathrm{i}2\pi(hx_j + ky_j + lz_j)] \tag{3.63}$$

The *structure factor* F(*hkl*) is a dimensionless scalar quantity and refers to the combined scattering from the *n* atoms in the unit cell to give the *hkl* spectrum, or equally to the wave from the (*hkl*) family of planes, relative to the scattering by a single electron at the origin; see also Sect. 3.2.3. The atomic scattering factor $f_{j,\theta}$ for the *j*th atom indicates its dependence on θ, an alternative parameter to **S** in this context. Again, frequently the θ dependence of f is not expressed in the formula, although it is implicitly always present. The atomic coordinates in (3.63) are fractional values, Sect. 2.2.3, and so are independent of the size of the unit cell.

3.6 Using the Structure Factor Equation

In the next two sections, we explore some of the properties and applications of the structure factor equation that are encountered in practical X-ray crystallography. The trigonometrical relations in Web Appendix WA5 may be helpful in some of the ensuing arguments.

3.6.1 Friedel's Law

Except where anomalous scattering is significant, Sect. 7.6, X-ray diffraction spectra form a centrosymmetric array. The diffraction spectra from a crystal may be thought of as an expression of its reciprocal lattice, with each spectrum *hkl* weighted by the corresponding value of the amplitude |F(*hkl*)|, or the intensity *I*(*hkl*). Friedel's law expresses the centrosymmetric property as

$$I(hkl) = I(\bar{h}\,\bar{k}\,\bar{l}) \quad \text{or} \quad |\mathrm{F}(hkl)| = |\mathrm{F}(\bar{h}\,\bar{k}\,\bar{l})| \tag{3.64}$$

within the limits of experimental error, and may be derived as follows.

Since the atomic scattering factor is a function of $(\sin\theta)/\lambda$, it will have the same value for both the *hkl* and $\bar{h}\,\bar{k}\,\bar{l}$ reflections. Thus, $f_\theta = f_{-\theta}$, because reflections from opposite sides of any plane occur at the same value of the Bragg angle θ.

From (3.63)

$$\mathrm{F}(\bar{h}\,\bar{k}\,\bar{l}) = \sum_{j=1}^{n} f_j \exp[-\mathrm{i}2\pi(hx_j + ky_j + lz_j)] \tag{3.65}$$

and from Fig. 3.13

$$\mathrm{F}(hkl) = A'(hkl) + \mathrm{i}B'(hkl)\mathrm{F}(\bar{h}\,\bar{k}\,\bar{l}) = A'(\bar{h}\,\bar{k}\,\bar{l}) + \mathrm{i}B'(\bar{h}\,\bar{k}\,\bar{l}) = A'(hkl) - \mathrm{i}B'(hkl) \tag{3.66}$$

Hence, the following relations hold:

$$\phi(hkl) = -\phi(\bar{h}\,\bar{k}\,\bar{l})|\mathrm{F}(hkl)| = |\mathrm{F}(\bar{h}\,\bar{k}\,\bar{l})| = [A'^2(hkl) + B'^2(hkl)]^{1/2} \tag{3.67}$$

and, since $I = |\mathrm{F}|^2$

$$I(hkl) = I(\bar{h}\,\bar{k}\,\bar{l}) \tag{3.68}$$

which is Friedel's law.

3.6.2 Structure Factor for a Centrosymmetric Crystal

One of the questions that frequently arises at the outset of a crystal structure determination is whether or no the space group is centrosymmetric. In a centrosymmetric structure, with the origin on a center of symmetry, the n atoms in the unit cell lie in related pairs, with coordinates $\pm(x, y, z)$. From (3.18) and (3.19), we write for the two parts of the structure factor equation:

$$\begin{aligned} A'(hkl) &= \sum_{j=1}^{n/2} f_j[\cos 2\pi(hx_j + ky_j + lz_j) + \cos 2\pi(-hx_j - ky_j - lz_j)] \\ &= 2\sum_{j=1}^{n/2} f_j \cos 2\pi(hx_j + ky_j + lz_j) \end{aligned} \tag{3.69}$$

where j ranges over the $n/2$ atoms in the unit cell *not* related by the center of symmetry.

For $B'(hkl)$, we write

$$B'(hkl) = \sum_{j=1}^{n/2} f_j[\sin 2\pi(hx_s + ky_s + lz_s) + \sin 2\pi(-hx_s - ky_s - lz_s)] = 0 \tag{3.70}$$

Here, $B' = 0$ because $\sin(-\phi) = -\sin(\phi)$ for all ϕ, in accord with (3.20). In this case, $A'(hkl) = F(hkl)$, and $\phi(hkl)$ can take only the values 0 or π, so that the phase angle attaches itself to $|\mathrm{F}(hkl)|$ as a positive or negative sign. Hence, we often speak of the *signs*, s, of reflections in centrosymmetric crystals, so that $\mathrm{F}(hkl) = s(hkl)\,|\mathrm{F}(hkl)|$. Clearly, these results apply only when the origin of the unit cell is taken on $\bar{1}$; in any other setting of the origin in a centrosymmetric space group, there will normally be a non-zero component in $B'(hkl)$. Centrosymmetric crystals usually present fewer

difficulties to the structure analyst than do non-centrosymmetric crystals because of the above restriction on the phase angles.

3.7 Limiting Conditions and Systematic Absences

We considered limiting conditions briefly in Sect. 2.7.1; here we investigate them more fully through the structure factor equation and show how they are handled in several different example symmetries.

An X-ray diffraction pattern can be used to determine the type of unit cell that corresponds to the chosen system of reference axes. From (3.63), it would be an unexpected coincidence for many intensities to be zero. With unit cells having no translational symmetry, the intensity of a reflection is not usually zero for any particular combinations of h, k, and l, that is, no *limiting conditions* apply in such a case. Vanishingly weak intensities may arise for certain reflections because of the particular structure under investigation; we call these reflections *accidental absences*, and we shall discuss them further, in Sect. 4.2.3. In centered unit cells or in the presence of other translational symmetry, glide planes and screw axes, reflections of certain combinations of h, k, and l are totally absent; we call such unobservable reflections *systematic absences*.

3.7.1 Body-Centered Unit Cell

As a first example, we know that in a body-centered (I) unit cell, the atoms are related in pairs as x, y, z and $\frac{1}{2}+x,\ \frac{1}{2}+y,\ \frac{1}{2}+z$. Using (3.63), we have

$$\mathrm{F}(hkl) = \sum_{j=1}^{n/2} f_j \{\exp[\mathrm{i}2\pi(hx_j + ky_j + lz_j)] + \exp[\mathrm{i}2\pi(hx_j + ky_j + lz_j + h/2 + k/2 + l/2)]\} \quad (3.71)$$

The term within the braces $\{\ldots\}$ may be expressed as $\exp[\mathrm{i}2\pi(hx_j + ky_j + lz_j)]\{1 + \exp[\mathrm{i}2\pi(h+k+l)/2]\}$. Since $h + k + l$ is integral, $\{1+ \exp[\mathrm{i}2\pi(h+k+l)/2]\} = 1 + \cos[2\pi(h+k+l)/2] = 2\cos^2[2\pi(h+k+l)/4] = G$, where G is a multiplying factor for the *reduced* structure factor equation in centered unit cells; in the body-centered unit cell $G = 2$, so that

$$\mathrm{F}(hkl) = 2\cos^2[2\pi(h+k+l)/4] \sum_{j=1}^{n/2} f_j \exp[\mathrm{i}2\pi(hx_j + ky_j + lz_j)] \quad (3.72)$$

This equation may be broken down into its two components, $A'(hkl)$ and $B'(hkl)$, in the usual way. Further simplification is possible: in this example, G takes the value 2 if $h + k + l$ is even, and 0 if $h + k + l$ is odd. Hence, we write the *limiting condition* that shows which reflections are *permitted* by the geometry of an I unit cell as

$$hkl : h + k + l = 2n, \quad n = 0, \pm 1, \pm 2, \ldots$$

The same situation expressed as *systematic absences*, the condition under which reflections are *forbidden* by the space-group geometry, is

$$hkl : h + k + l = 2n + 1, \quad n = 0, \pm 1, \pm 2, \ldots$$

Both terms are in common use, and the reader should distinguish between them. We could have reached the same conclusion from (3.71) more speedily: the expression $\{1 + \exp[i2\pi(h + k + l)/2]\}$ is equal to $1 + \exp(i\pi n)$, where n is the sum of the integers h, k, and l, and $[1 + \exp(i\pi n)]$ is 2 or 0 for n even or odd. But it is preferable to highlight the dependence on h, k, and l.

Analogous expressions can be derived for any centered unit cell. The G factors for all types of centering have been summarized in Table 3.2. It is evident that where a reflection arises in a centered unit cell, the structure factor equation has the same form as that for the corresponding primitive unit cell, but multiplied by the G factor appropriate to the unit cell type. The summation in the reduced structure factor equation is then taken over that fraction of atoms *not* related by the centering symmetry.

In practice, the diffraction pattern is recorded, indices allocated to the spectra and then scrutinized for systematic absences, so as to determine the unit cell type. The reader may care to work through the derivations of F(hkl) for, say, a C and an F unit cell, and determine the limiting conditions for each unit cell type; see also Sect. 3.8.

3.7.2 Screw Axes and Glide Planes

As we are concerned in this discussion with the geometry of the unit cell rather than the chemical nature of its contents, it is convenient to introduce the following nomenclature. Let N be the total number of atoms in the unit cell, and let n of them be the number in the asymmetric unit, with the number of asymmetric units being m, so that $N = nm$. Symbolically, we may write

$$\sum_{j=1}^{N} \equiv \sum_{r=1}^{n} \sum_{s=1}^{m}$$

where the sum over r refers to the symmetry-independent atoms, and that over s to the symmetry-related species. Thus, the structure factor equation contains two parts that may be considered separately. The sum over m symmetry-related atoms is expressed through the coordinates of a set of general equivalent positions. Thus,

$$\begin{aligned} A_r(hkl) &= \sum_{s=1}^{m} \cos 2\pi(hx_s + ky_s + lz_s) \\ B_r(hkl) &= \sum_{s=1}^{m} \sin 2\pi(hx_s + ky_s + lz_s) \end{aligned} \tag{3.73}$$

Extending to the n atoms in the asymmetric unit, with one such term for each atom,

$$\begin{aligned} A'(hkl) &= \sum_{r=1}^{n} f_r A_r(hkl) \\ B'(hkl) &= \sum_{r=1}^{n} f_r B_r(hkl) \end{aligned} \tag{3.74}$$

The terms $A_r(hkl)$ and $B_r(hkl)$ are independent of the nature and arrangement of the atoms in the asymmetric unit; they are a property of the space-group symmetry and are called *geometrical*

structure factors. We shall consider some examples taken from the monoclinic and orthorhombic systems, in order to show how glide-plane and screw-axis symmetries give rise to limiting conditions with special classes of reflections. For this discussion, the subscript s in (3.73) need not be retained, because all m positions are related to the position x, y, z by symmetry, and in the geometrical structure factors we shall, for simplicity, drop the subscript r.

Space Group $P2_1$

General equivalent positions: $x, y, z;\ \bar{x}, \frac{1}{2}+y, \bar{z}$, see Fig. 2.30.

Geometrical structure factors:

$$\begin{aligned} A(hkl) &= \cos 2\pi(hx+ky+lz) + \cos 2\pi(-hx+ky-lz+k/2) \\ &= 2\cos 2\pi(hx+lz-k/4)\cos 2\pi(ky+k/4) \end{aligned} \tag{3.75}$$

In a similar way,

$$\begin{aligned} B(hkl) &= \sin 2\pi(hx+ky+lz) + \sin 2\pi(-hx+ky-lz+k/2) \\ &= 2\cos 2\pi(hx+lz-k/4)\sin 2\pi(ky+k/4) \end{aligned} \tag{3.76}$$

Limiting Conditions in $P2_1$

Geometrical structure factors enable us to determine limiting conditions, that is, to predict which classes of reflections are capable of arising in an X-ray diffraction pattern. If we can show, for given values of h, k, and l, that both $A(hkl)$ and $B(hkl)$ are systematically zero, then F(hkl) will be zero, regardless of the atomic positions.

For $P2_1$, we can cast (3.75) and (3.76) in the following forms, according to the parity (evenness or oddness) of k. Expanding (3.75), we have (see Web Appendix WA5):

$$\begin{aligned} A(hkl)/2 = {} & [\cos 2\pi(hx+lz) + \cos 2\pi(k/4) + \sin 2\pi(hx+lz)\ \sin 2\pi(k/4)] \\ & \times [\cos 2\pi(ky)\ \cos 2\pi(k/4) - \sin 2\pi(ky)\ \sin 2\pi(k/4)] \end{aligned} \tag{3.77}$$

In expanding the right-hand side of (3.77), terms such as

$$\cos 2\pi(hx+lz)\cos 2\pi(k/4)\sin 2\pi(ky)\sin 2\pi(k/4)$$

occur. This particular term is equivalent to

$$\frac{1}{2}\cos 2\pi(hx+lz)\ \sin 2\pi(ky)\ \sin 4\pi(k/4)$$

which is zero, because k is an integer. Hence, (3.77) becomes

$$\begin{aligned} A(hkl)/2 = {} & [\cos 2\pi(hx+lz)\cos 2\pi(ky)\cos^2 2\pi(k/4)] - [\sin 2\pi(hx+lz) \\ & \times \sin 2\pi(ky)\sin^2 2\pi(k/4)] \end{aligned} \tag{3.78}$$

In a similar manner, we find from (3.76)

$$\begin{aligned} B(hkl)/2 = {} & [\cos 2\pi(hx+lz)\ \sin 2\pi(ky)\cos^2 2\pi(k/4)] + [\sin 2\pi(hx+lz) \\ & \times \cos 2\pi(ky)\sin^2 2\pi(k/4)] \end{aligned} \tag{3.79}$$

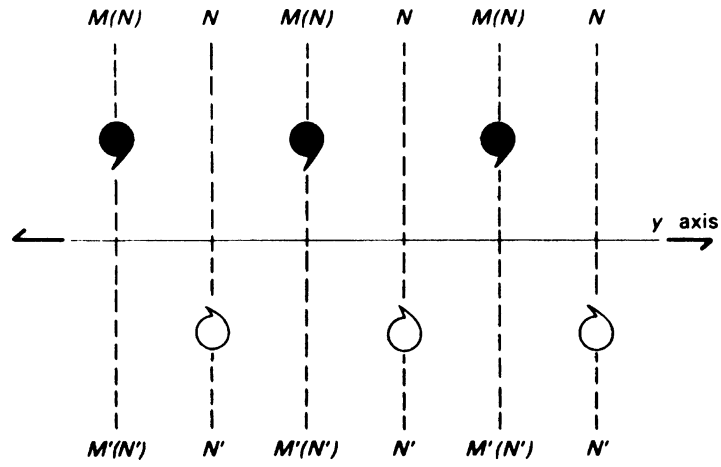

Fig. 3.22 Pattern of a structure containing a 2_1 screw axis: $d(NN') = d(MM')/2$, so that the MM' planes are *halved* by the NN' family

Separating for k even and k odd, we obtain

$$k = 2n: A(hkl) = 2\cos 2\pi(hx + lz)\cos 2\pi(ky) \tag{3.80}$$

$$B(hkl) = 2\cos 2\pi(hx + lz)\ \sin 2\pi(ky) \tag{3.81}$$

$$k = 2n + 1: A(hkl) = -2\sin 2\pi(hx + lz)\ \sin 2\pi(ky) \tag{3.82}$$

$$B(hkl) = 2\sin 2\pi(hx + lz)\ \cos 2\pi(ky) \tag{3.83}$$

Only one systematic condition can be extracted from these equations: if both h and l are zero, then from (3.82) and (3.83).

$$A(hkl) = B(hkl) = 0$$

In other words, the limiting conditions associated with a 2_1 axis are

hkl	None (P unit cell)
$0k0$	$k = 2n$

The example of the 2_1 axis has been treated in detail; it shows again how a diffraction record may be used to reveal information about the translational symmetry elements of a space group. We can show how the limiting conditions for a 2_1 axis arise from a consideration of the Bragg equation. Figure 3.22 is a schematic illustration of a 2_1 symmetry pattern; the motif represents a structure at a height z, and the structure at a height $\bar{z}$ after operating on it with the 2_1 axis. The planes MM' represent the family $(0k0)$ and NN' the family $(02k,0)$.

Reflections of the type $(0k0)$ from MM' planes are canceled by the reflections from the NN' planes, because their phase change relative to MM' is 180°. Clearly, this result is not obtained with the $02k,0$ reflections. Although the figure illustrates the situation for $k = 1$, the same argument can be applied to any pair of values k and $2k$, where k is an odd integer. Limiting conditions for other screw axes, and in other orientations, can be deduced as above, and the results are summarized in Table 3.3. Notice that pure rotation axes, as in space group $P2$, do not introduce any limiting conditions.

Table 3.3 Limiting conditions for screw axes

Screw axis	Orientation	Limiting condition	Translational component
2_1	$\parallel x$	$h00$: $h = 2n$	$a/2$
2_1	$\parallel y$	$0k0$: $k = 2n$	$b/2$
2_1	$\parallel z$	$00l$: $l = 2n$	$c/2$
3_1 or 3_2	$\parallel z$	$000l$: $l = 3n$	$c/3$ or $2c/3$
4_1 or 4_3	$\parallel z$	$00l$: $l = 4n$	$c/4$ or $3c/4$
4_2	$\parallel z$	$00l$: $l = 2n$	$2c/4$ ($c/2$)
6_1 or 6_5	$\parallel z$	$000l$: $l = 6n$	$c/6$ or $5c/6$
6_2 or 6_4	$\parallel z$	$000l$: $l = 3n$	$2c/6$ ($c/3$), $c/6(2c/3)$
6_3	$\parallel z$	$000l$: $l = 2n$	$3c/6$ ($c/2$)

In the cubic system, 4_1, 4_3, and 4_2 axes parallel to x and y exhibit limiting conditions similar to those parallel to z by cyclic permutation

Centric Zones

Centric zones, sometimes loosely termed centrosymmetric zones, are of particular importance in crystal structure determination; see also Sect. 4.2.3. In space group $P2_1$ and other space groups of crystal class 2, the $h0l$ reflections are of special interest. Among (3.80)—(3.83), only (3.80) is relevant here because zero behaves as an even number, and $\sin(2\pi ky)_{k=0} = 0$. Hence,

$$A(h0l) = 2\cos 2\pi(hx + lz) \quad B(h0l) = 0 \tag{3.84}$$

From (3.20), $\phi(h0l)$ is either 0 or π; in other words, the [010] zone is centric for this space group. Centric zones occur in the non-centrosymmetric space groups that have symmetry 2 as a subgroup of their point groups; see Sects. 1.4.2 and 2.7.3ff.

Space Group *Pc*

General equivalent positions: x, y, z; $x, \bar{y}, \frac{1}{2} + z$.

Geometrical structure factors: Proceeding as before, we obtain

$$\begin{aligned} A(hkl) &= 2\cos 2\pi(hx + lz + l/4)\ \cos 2\pi(ky - k/4) \\ B(hkl) &= 2\sin 2\pi(hx + lz + l/4)\ \cos 2\pi(ky - l/4) \end{aligned} \tag{3.85}$$

If we expand these equations, as with the example for $P2_1$, and then separate the terms for l even and l odd, we shall find systematic absences only for the $h0l$ reflections. Thus, the limiting conditions for Pc are

hkl	None
$h0l$	$l = 2n$

The relationship between the index (l) involved in the condition and the symmetry translation ($c/2$) is clear. A space group diagram for Pc is shown in Fig. 3.23.

Space Group $P2_1/c$

This space group contains the two translational symmetry operations already discussed, namely, a 2_1 axis parallel to y and a c-glide normal to y, Fig. 2.32 and Problem 2.8a. It is a centrosymmetric space group, and the general equivalent positions may be summarized as

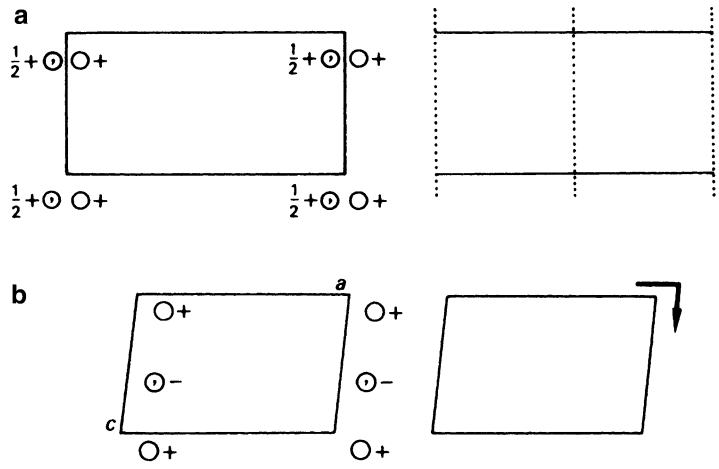

Fig. 3.23 Space group *Pc*. (**a**) Viewed along *c*. (**b**) Viewed along *b*

$$\pm\{x, y, z; x, \tfrac{1}{2} - y, \tfrac{1}{2} + z\}$$

Geometrical structure factors: In the standard setting of this space group, the origin is on $\bar{1}$, so that we can immediately apply (3.69) and (3.70) and write

$$A(hkl) = 2\{\cos 2\pi[hx + ky + lz] + \cos 2\pi[hx - ky + lz + (k + l)/2]\}B(hkl) = 0 \tag{3.86}$$

Combining the two cosine terms

$$A(hkl) = 4\cos 2\pi[hx + lz + (k + l)/4]\cos 2\pi[ky - (k + l)/4)]$$

Separating for $k + l$ even and odd, we obtain

$$\begin{aligned} k + l &= 2n, \quad & A(hkl) &= 4\cos 2\pi(hx + lz)\cos 2\pi(ky) \\ k + l &= 2n + 1, \quad & A(hkl) &= -4\sin 2\pi(hx + lz)\sin 2\pi(ky) \end{aligned} \tag{3.87}$$

We now deduce the limiting conditions as

hkl	None
*h*0*l*	$l = 2n$ (*c*-glide normal to *y*)
0*k*0	$k = 2n$ (2_1 axis $\parallel$ *y*)

These three classes of reflections are important in monoclinic reciprocal space, because only with *them* can we determine the characteristic systematic absences in the space groups within this system. Despite Friedel's law, the diffraction symmetry reveals the true space group in this example. Figure 3.24 illustrates weighted reciprocal space levels for a monoclinic crystal of space group *Pc*, $P2/c$, or $P2_1/c$.

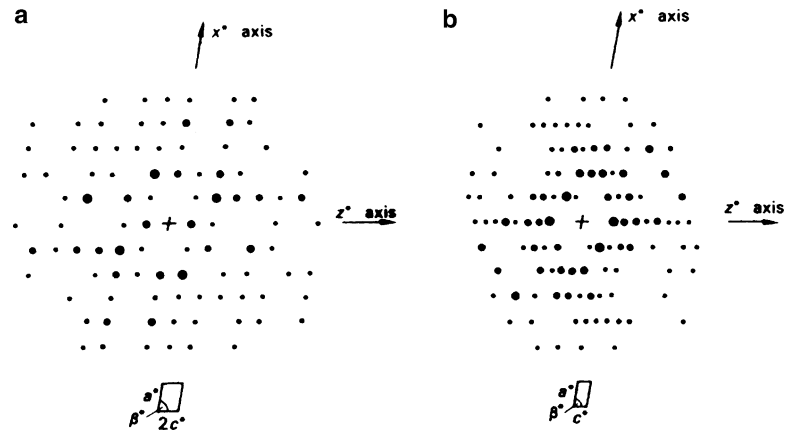

Fig. 3.24 Reciprocal nets in the x^*, z^* plane appropriate to space groups Pc, $P2/c$, and $P2_1/c$. (**a**) $k = 0$ and (**b**) $k > 0$. The c-glide plane, which is perpendicular to b, causes a halving of the rows parallel to x^* when $k = 0$, so that only the rows with $l = 2n$ are present. Hence, the true c^* spacing is not observed on the reciprocal lattice level $k = 0$, but can be determined from higher levels. The symmetry on both levels is 2, in accordance with the diffraction symmetry $2/m$: $|\mathrm{F}(hkl)| = |\mathrm{F}(\bar{h}\,\bar{k}\,\bar{l})|$. The reciprocal lattice points are weighted according to $|\mathrm{F}(hkl)|$, or to $|\mathrm{F}(hkl)|^2$, and we speak of such diffraction patterns as *weighted reciprocal lattices*

Space Group *Pma*2

From the data in Fig. 3.25 we can write down expressions for the geometrical structure factors:

$$A(hkl) = \cos 2\pi(hx + ky + lz) + \cos 2\pi(-hx - ky + lz) + \cos 2\pi(-hx + ky + lz + h/2) + \cos 2\pi(hx - ky + lz + h/2) \tag{3.88}$$

Combining the first and third, and second and fourth terms, we have

$$A(hkl) = 2\cos 2\pi(ky + lz + h/4) + \cos 2\pi(hx - h/4) + 2\cos 2\pi(-ky + lz + h/4) \times \cos 2\pi(hx + h/4) \tag{3.89}$$

Further simplification of this expression requires the separate parts to contain a common factor. We return to (3.88) and make a minor alteration to the term $\cos 2\pi(hx - ky + lz + h/2)$. Since h is an integer, we may write this term as the crystallographically equivalent term $\cos 2\pi(hx - ky + lz - h/2)$. Another way of looking at this process is that the fourth general equivalent position has been changed to $-\frac{1}{2} + x, \bar{y}, z$, which is equivalent to moving through one repeat a in the negative direction to a crystallographically equivalent position, a perfectly valid and generally applicable tactic.

Returning to *Pma*2, (3.89) now becomes

$$A(hkl) = 2\cos 2\pi(ky + lz + h/4)\cos 2\pi(hx - h/4) + 2\cos 2\pi(-ky + lz - h/4)\cos 2\pi(hx - h/4) \tag{3.90}$$

which simplifies to

$$A(hkl) = [2\cos 2\pi(hx - h/4)][\cos 2\pi(ky + lz + h/4) + \cos 2\pi(-ky + lz - h/4)] \tag{3.91}$$

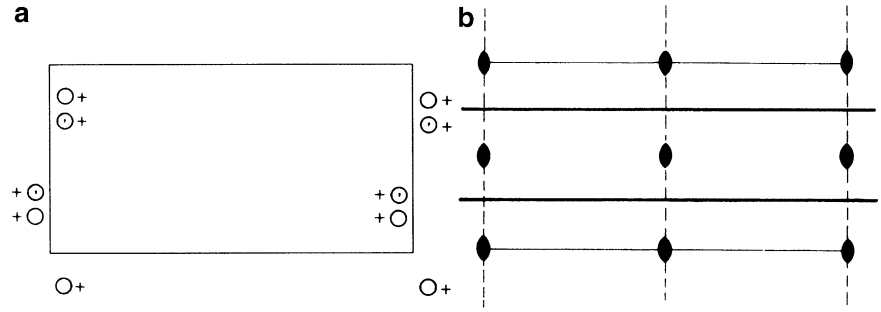

Origin on 2

							Limiting conditions
4	*d*	1	x, y, z;	$\bar{x}, \bar{y}, z$;	$\frac{1}{2}-x, y, z$;	$\frac{1}{2}+x, \bar{y}, z$.	*hkl*: None 0*kl*: None *h*0*l*: $h = 2n$ *hk*0: None *h*00: $(h = 2n)$ 0*k*0: None 00*l*: None
2	*c*	*m*	$\frac{1}{4}, y, z$;	$\frac{3}{4}, \bar{y}, z$.			As above
2	*b*	2	$0, \frac{1}{2}, z$;	$\frac{1}{2}, \frac{1}{2}, z$.			As above +
2	*a*	2	$0, 0, z$;	$\frac{1}{2}, 0, z$.			*hkl*: $h = 2n$

Symmetry of special projections

(001) *p*2*mg* (100) *pm*1 (*p*1*m*1) (010) *p*1*m* (*p*11*m*) $a' = a/2$

Fig. 3.25 General equivalent positions and symmetry elements in space group *Pma*2, with the origin on 2; the origin is not fixed in the z direction by the symmetry elements. The diagram shows inter alia the coordinates of the special equivalent positions and the limiting conditions

Combining again:

$$A(hkl) = 4[\cos 2\pi(hx - h/4)] \cos 2\pi(ky + h/4) \cos 2\pi lz \tag{3.92}$$

Similarly,

$$B(hkl) = 4[\cos 2\pi(hx - h/4)] \cos 2\pi(ky + h/4) \sin 2\pi lz \tag{3.93}$$

In the orthorhombic system, seven regions of reciprocal space of particular importance are listed on the right-hand side of Fig. 3.25. Separating (3.92) and (3.93) for even and odd values of h, we obtain

$$\begin{aligned} h = 2n: \quad A(hkl) &= 4 \cos 2\pi hx \cos 2\pi ky \cos 2\pi lz \\ B(hkl) &= 2 \cos 2\pi hx \cos 2\pi ky \sin 2\pi lz \end{aligned} \tag{3.94}$$

$$\begin{aligned} h = 2n+1: \quad A(hkl) &= -4 \sin 2\pi hx \sin 2\pi ky \cos 2\pi lz \\ B(hkl) &= -4 \sin 2\pi hx \sin 2\pi ky \sin 2\pi lz \end{aligned} \tag{3.95}$$

from which we find the limiting conditions

hkl	None
*h*0*l*	$h = 2n$

Table 3.4 Limiting conditions for glide planes

Glide plane	Orientation	Limiting condition	Translational component
a	$\perp b$	$h0l$: $h = 2n$	$a/2$
a	$\perp c$	$hk0$: $h = 2n$	$a/2$
b	$\perp a$	$0kl$: $k = 2n$	$b/2$
b	$\perp c$	$hk0$: $k = 2n$	$b/2$
c	$\perp a$	$0kl$: $l = 2n$	$c/2$
c	$\perp b$	$h0l$: $l = 2n$	$c/2$
n	$\perp a$	$0kl$: $k + l = 2n$	$(b + c)/2$
n	$\perp b$	$h0l$: $l + h = 2n$	$(c + a)/2$
n	$\perp c$	$hk0$: $h + k = 2n$	$(a + b)/2$
d	$\perp a$	$0kl$: $k + l = 4n$ ($k, l = 2n$)	$(b \pm c)/4$
d	$\perp b$	$h0l$: $l + h = 4n$ ($l, h = 2n$)	$(c \pm a)/4$
d	$\perp c$	$hk0$: $h + k = 4n$ ($h, k = 2n$)	$(a \pm b)/4$

The listed condition $h00$: $(h = 2n)$ should be considered carefully. One might be excused for thinking at first that it implies the existence of a 2_1 axis parallel to the x axis, but for the knowledge that there are no symmetry axes parallel to the x axis in class $mm2$. This particular limiting condition is dependent upon the $h0l$ condition: $h00$ is in the $h0l$ zone.

We emphasize here that confusion can very easily arise if the limiting conditions are interpreted in other than the following hierarchal order:

Order of inspection Downward	
hkl	Unit cell type
$0kl$	Glide plane $\perp x$
$h0l$	Glide plane $\perp y$
$hk0$	Glide plane $\perp z$
$h00$	2_1 axis $\parallel x$
$0k0$	2_1 axis $\parallel y$
$00l$	2_1 axis $\parallel z$

One should proceed to a lower level in this list only after considering the full implications of the conditions at higher levels. Conditions such as that for $h00$ in $Pma2$ are called *redundant* or *dependent* and are placed in parentheses on the diagram. Reflections involved in such conditions are certainly absent from a diffraction record, but do not contribute to the determination of space-group symmetry. Table 3.4 summarizes the limiting conditions for glide-plane symmetry.

Space Group *Pman*

This space group may be derived from $Pma2$ by the addition of an n-glide plane perpendicular to the z axis, with a translational component of $(a + b)/2$. We have now seen on several occasions that it is advantageous to set the origin at $\bar{1}$ wherever possible; Fig. 3.26 shows $Pman$ drawn in this orientation. It is left to the reader to show that the geometrical structure factors are

$$\begin{aligned} A(hkl) &= 8\cos 2\pi hx \cos 2\pi[ky - (h+k)/4]\cos 2\pi[lz + (h+k)/4] \\ B(hkl) &= 0 \end{aligned} \tag{3.96}$$

and subsequently to derive the limiting conditions for this space group.

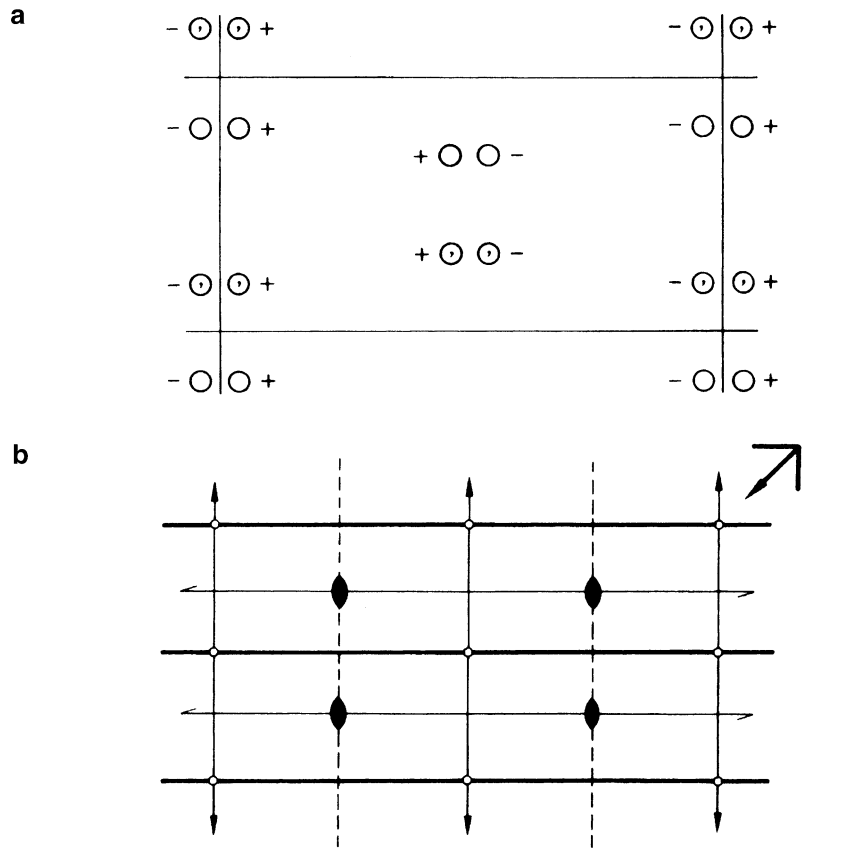

$\pm\{x, y, z;\quad \bar{x}, y, z;\quad \frac{1}{2}+x, \frac{1}{2}-y, z;\quad \frac{1}{2}-x, \frac{1}{2}-y, z\}$

Limiting conditions

hkl:	None
$0kl$:	None
$h0l$:	$h = 2n$
$hk0$:	$h + k = 2n$
$h00$:	$(h = 2n)$
$0k0$:	$(k = 2n)$
$00l$:	None

Fig. 3.26 Space group *Pman*. (**a**) General equivalent positions. (**b**) Symmetry elements; the origin is on $\bar{1}$. The diagram shows also the limiting conditions for this space group.

Space Group $P6_3/m$

Finally here, and in order to show that these manipulations are fundamentally no more difficult with a space group not based on orthogonal axes, we study the hexagonal space group $P6_3/m$; we will address the tetragonal system through space group $P4nc$ in a problem.

From Fig. 2.38, we list the coordinates as:

$$\pm\{x, y, z; \bar{y}, x-y, z; \bar{x}+y, \bar{x}, z; \bar{x}, \bar{y}, \tfrac{1}{2}+z; y, \bar{x}+y, \tfrac{1}{2}+z; x-y, x, \tfrac{1}{2}+z\}$$

Since the structure is centrosymmetric, with the origin on $6/m\ (\bar{1})$, we need consider only the cosine part of the structure factor equation ($B = 0$). Thus, following (3.69) we can write the geometrical structure factor as:

$$\begin{aligned} A/2 = {} & \cos 2\pi(hx + ky + lz) + \cos 2\pi(-hy + k[x - y] + lz) + \cos 2\pi(h[y - x] - kx + lz) \\ & + \cos 2\pi(-hx - ky + lz + l/2) + \cos 2\pi(hy + k[y - x] + lz + l/2) \\ & + \cos 2\pi(h[x - y] + kx + lz + l/2) \end{aligned}$$

Combining the cosine terms in pairs, we obtain

$$\begin{aligned} A/4 = {} & \cos 2\pi(lz - l/4)\{\cos 2\pi(hx + ky + l/4) + \cos 2\pi(kx + iy + l/4) \\ & + \cos 2\pi(ix + hy + l/4)\} \end{aligned}$$

[remember that $i = -(h + k)$]. We can now separate into equations for l even and l odd by expanding the cosine terms (you may need Web Appendix WA5):

$$\begin{aligned} l = 2n: \qquad & A = 4\cos 2\pi lz\{\cos 2\pi(hx + ky) + \cos 2\pi(kx + iy) + \cos 2\pi(ix + hy)\} \\ l = 2n + 1: \qquad & A = -4\sin 2\pi lz\{\sin 2\pi(hx + ky) + \sin 2\pi(kx + iy) + \sin 2\pi(ix + hy)\} \end{aligned}$$

For l even, there are no reflection conditions; for l odd, $A = 0$ if $h = k = 0$. Thus, the only condition limiting X-ray reflections is $000l = l = 2n$. The expression above for $A/2$ differs in a trivial manner from that given in the International Tables [10]: the value therein may be achieved by using initially the crystallographically equivalent position $(-\frac{1}{2} + z)$, in place of the $\frac{1}{2} + z$ employed here.

3.8 Practical Determination of Space Groups from Diffraction Data

The determination of the space group of a crystal is an important and early feature in the X-ray analysis of its structure. We shall assume that we have available the X-ray diffraction record for the several examples of monoclinic and orthorhombic crystals to be examined. It is necessary to bear in mind that X-ray techniques can reveal the presence of that translational symmetry which can arise through symmetry operations:

1. Translations relating to centering of the unit cell ($a/2$ and/or $b/2$ and/or $c/2$).
2. Translations relating to glide planes.
3. Translations relating to screw axes.

or any combination of these symmetry operations. All categories lead to systematic absences, and the totality of the translational symmetry, together with the Laue group, forms the diffraction symbol, Sect. 2.9.

Table 3.5 Some reflection data for monoclinic crystal I

hkl	200	401	112	510
	201	402	113	020
	202	600	114	040
	203	110	310	060
	400	111	311	080

Table 3.6 Some reflection data for monoclinic crystal II

hkl	100	204	111	322
	200	402	122	020
	300	502	113	040
	400	110	311	060
	202	310	123	080

Table 3.7 Limiting conditions for the monoclinic space groups

Conditions limiting possible X-ray reflections	Space groups
hkl: none $h0l$: none $0k0$: none	$P2$, Pm, $P2/m$
hkl: none $h0l$: none $0k0$: $k = 2n$	$P2_1$, $P2_1/m$
hkl: none $h0l$: $l = 2n$ $0k0$: none	Pc, $P2/c$
hkl: none $h0l$: $l = 2n$ $0k0$: $k = 2n$	$P2_1/c$
hkl: $h + k = 2n$ $h0l$: none $0k0$: none	$C2$, Cm, $C2/m$
hkl: $h + k = 2n$ $h0l$: $l = 2n (h = 2n)$ $0k0$: none	Cc, $C2/c$

3.8.1 Monoclinic Space Groups

Single crystal X-ray photographs taken with a monoclinic crystal showed typically the reflections listed in Table 3.5.

From the important reflection types, hkl, $h0l$, and $0k0$, we deduce the limiting conditions:

hkl	$h + k = 2n$
$h0l$	$(h = 2n)$
$0k0$	$(k = 2n)$

Using Table 3.7, we conclude that for crystal I, the space group is one of $C2$, Cm, or $C2/m$. The diffraction data alone do not distinguish between these three possible space groups; we show in Sect. 4.2.3ff how this ambiguity might be resolved.

Table 3.6, for monoclinic crystal II, provides the next list of diffraction data for inspection.

Table 3.8 Some reflection data for an orthorhombic crystal

hkl				
	111	011	110	020
	112	021	120	040
	212	012	310	060
	312	101	200	002
	322	203	400	004
	332	303	600	006

There is no condition on *hkl*, but *h*0*l* are restricted by *l* being even, and 0*k*0 by *k* being even: this space group is identified uniquely as $P2_1/c$.

The limiting conditions for the 13 monoclinic space groups are listed in Table 3.7, in their standard orientations. In practice, it is possible, by an inadvertent choice of axes, to find oneself working with a non-standard space-group symbol. Generally, a fairly straightforward transformation of axes will lead to the standard setting (see Problems 2.12 and 3.17).

3.8.2 Orthorhombic Space Groups

We begin with the sample data in Table 3.8. From these data, we deduce the conditions below:

Limiting conditions deduced:

hkl	None	*h*00	$h = 2n$
0*kl*	None	0*k*0	$k = 2n$
*h*0*l*	None	00*l*	$l = 2n$
*hk*0	None		

Examining in the prescribed hierarchy, we find only 2_1 axes parallel to *x*, *y*, and *z*: the space group is determined uniquely as $P2_12_12_1$, Sect. 2.7.7 and Table 2.7.

In the final two examples, we consider only the conclusions drawn from an inspection of the diffraction records. In the first instance, we have:

hkl	None	*h*00	None
0*kl*	$k = 2n$	0*k*0	$(k = 2n)$
*h*0*l*	$l = 2n$	00*l*	$(l = 2n)$
*hk*0	None		

The diffraction symbol is *mmm Pbc*$*$ so that the space group is either $Pbc2_1$ or *Pbcm*; the distinction between them depends upon the presence, or otherwise, of a center of symmetry.

In the second example, we have:

hkl	None	*h*00	$(h = 2n)$
0*kl*	$k = 2n$	0*k*0	$(k = 2n)$
*h*0*l*	$l = 2n$	00*l*	$(l = 2n)$
*hk*0	$h = 2n$		

and space group *Pbca* is uniquely determined.

These results seem quite reasonable and straightforward, but nevertheless, one might be tempted to question their validity. For example, in the first orthorhombic crystal, is there a space group in class *mmm* that would give the same systematic absences as those in Table 3.8? Experience tells us that there is not. Since no glide planes are indicated by the systematic absences, the three symmetry planes, if present, would have to be *m*-planes. Three *m*-planes could not be involved with three 2_1

axes unless the unit cell were centered, for example, as in *Immm*, which would restrict the *hkl* reflections to $h + k + l = 2n$. Hence, our original conclusion is correct.

3.8.3 Tetragonal Space Groups

The following reflections conditions were obtained for two tetragonal crystals of Laue groups $\frac{4}{m}mm$ and $\frac{4}{m}$, respectively. It may help to consider again Table 1.5.

(a) hkl : none $\quad hk0 : h + k = 2n \quad 0kl : k = 2n$
$\quad\quad P \qquad\qquad n \perp z \qquad\qquad b \perp x$

Consulting the International Tables, Volume 1 (or Volume A) on diffraction symbols shows that this space group is $P\frac{4}{n}bm$.

(b) $hkl : h + k + l = 2n \quad hk0 : h, (k) = 2n \quad 00l : l = 4n$
$\quad\quad I \qquad\qquad\qquad a \perp z \qquad\qquad 4_1 \,||\, z$

This space group is $I\frac{4_1}{a}$.

3.8.4 Hexagonal Space Groups

The following reflections conditions were obtained for two hexagonal crystals of point groups (a) 622 and (b) either $\frac{6}{m}mm$ or $6mm$, respectively.

(a) $hkil$: none $\quad 000l : l = 6n$
$\quad\quad P \qquad\qquad 6_1$ or 6_5

The diffraction symbol is: $622\,P\,6_1(6_5) * *$; thus, the space group is either $P6_122$ or its enantiomorph $P6_522$.

(b) hkl : none $\quad h0\bar{h}l : l = 2n$
$\quad\quad P \qquad\qquad c \perp x, (y)$

If the point group is $\frac{6}{m}mm$, reference to the International Tables for diffraction symbol $\frac{6}{m}mmP{*}c{*}$ leads to the space group is $P\frac{6_3}{m}cm$, whereas if the point group is $6mm$, similar considerations indicate space group $P6_3cm$.

The practicing X-ray crystallographer is assisted by the information on space groups in Volume A (and the earlier Volume 1) of the *International Tables for Crystallography* [10].

Combined with a working knowledge of symmetry, these tables enable most symmetry situations arising in the course of a structure analysis to be treated correctly.

3.9 Problems

3.1. What is the change in wavelength of an X-ray photon scattered incoherently by a free electron at 45° to the forward direction of the incident beam? If the wavelength of the incident photon is 1 Å, what is the energy of the scattered photon?

3.2. Two identical coherent scattering centers are separated by the distance 2λ, and X-rays fall normally on to the line joining the two centers. For $2\theta = 0$ to 180° in steps of 30°, calculate the scattered amplitudes and intensities as fractions of the results with both scatterers at one point.

3.3. Calculate the atomic scattering factor f for beryllium at $(\sin\theta)/\lambda = 0.0$, 0.2, and 0.5. The expression for $f(1s)$ has been given in the text. The Slater wave function for the $2s$ electron may be given as $\Psi_{2s} = (c_2^5/\ 96\pi)^{1/2} r \exp(c_2 r/2)$; you may need the general result $\int_0^\infty x^n \exp(-ax)\ \sin bx\ \ \mathrm{d}x = n![(a+\mathrm{i}b)^{n+1} - (a-\mathrm{i}b)^{n+1}]/[2\mathrm{i}(a^2+\ b^2)^{n+1}]$, from which the similar expression given in the text for the $1s$ wavefunction applies for the case $n = 1$. The screening constants for beryllium are $\sigma_{1s} = 0.3$ and $\sigma_{2s} = 2.05$. Compare the results that are obtained for f with those from the expression $f = \sum_j^4 a_j \exp(-b_j s^2) + c$, where s is $(\sin\theta)/\lambda$ and the values of a, b, and c for beryllium are listed below:

a_1	b_1	a_2	b_2	a_3	b_3	a_4	b_4	c
1.5919	43.6427	1.1278	1.8623	0.5391	103.483	0.7029	0.5420	0.0385

3.4. An X-ray tube is operated at 30 kV. What is the energy, in J, associated with each X-ray photon produced by the tube?

3.5. Calculate the transmittance factor (I/I_0) for a 1 mm crystal plate of benzene (C_6H_6), the density of which is 1,124 kg m^{-3}. The mass absorption coefficient for Cu $K\alpha$ X-radiation and the relative atomic masses are as follow:

	C	H
$\mu/m^2\ kg^{-1}$	0.46	0.04
M_r	12.01	1.008

3.6. There are eight combinations of one to three negative signs among the indices hkl for any general reflection. With the aid of the geometrical structure factors given in the text, derive the relationships between the eight forms of the phase angle $\phi(hkl)$ for (a) space group $P2_1$ and (b) space group $Pma2$.

3.7. A triclinic unit cell has the dimensions $a = 7.36$ Å, $b = 9.21$ Å, $c = 13.47$ Å, and $\alpha = 101.22°$, $\beta = 110.62°$, $\gamma = 123.41°$. Calculate (a) the six parameters of the reciprocal unit cell for Cu $K\alpha$ radiation ($\lambda = 1.5418$ Å), and (b) the volumes of the real and reciprocal unit cells.

3.8. In the direct unit cell of Problem 3.7, two atoms are situated at the fractional coordinates 0.10, 0.30, 0.20 and 0.10, 0.15, 0.35 for x, y, z, respectively. By means of vector expressions, calculate the distance between the two atoms, and the angle subtended at the origin by the vectors from the origin to each of the two atoms.

3.9. Three atoms have the following amplitudes and phases with respect to the real axis of an Argand diagram:
(a) 13.1, 16.23°
(b) 21.4, 154.87°
(c) 37.9, −113.26°
Calculate the amplitude and phase of the resultant sum.

3.10. Express the structure factor equation in a reduced form for an A-face centered unit cell. Hence, deduce the limiting conditions associated with A centering.

3.11. A two-dimensional structure has four atoms per unit cell, two of type P and two of type Q, with the following fractional coordinates:

	x	y
P_1	0.1	0.2
P_2	0.9	0.8
Q_1	0.2	0.7
Q_2	0.8	0.3

Calculate $|F(hk)|$ for the reflections 5 0, 0 5, 5 5 and 5 10 in terms of the scattering factors g_P and g_Q for the two species. If $g_P = 2g_Q$, what are the phase angles for these reflections?

3.12. α-Uranium crystallizes in the orthorhombic system with four uranium atoms in special positions:

$$\pm \{0, y, \tfrac{1}{4};\ \tfrac{1}{2}, \tfrac{1}{2} + y, \tfrac{1}{4}\}$$

Use the data below to decide whether y is better chosen as 0.10 or 0.15.

hkl	$\lvert F(hkl)\rvert$	$g_U(hkl)$
020	88.5	70.0
110	268.9	80.0

3.13. The unit cell dimensions of α-uranium are $a = 2.85$ Å, $b = 5.87$ Å, $c = 5.00$ Å. Use the value of y_U from Problem 3.12 to determine the shortest U–U distance in the structure. It may be helpful to plot the uranium atom positions in a few neighboring unit cells.

3.14. In the examples listed below for monoclinic crystals, the conditions limiting possible X-ray reflections are given. In each case, write the possible space groups corresponding to the information given.

(a)

hkl	None
$h0l$	None
$0k0$	$k = 2n$

(b)

hkl	None
$h0l$	$h = 2n$
$0k0$	None

(c)

hkl	$h + k = 2n$
$h0l$	$l = 2n$ ($h = 2n$)
$0k0$	($k = 2n$)

(d)

hkl	None
$h0l$	None
$0k0$	None

3.15. Repeat Problem 3.14, but for the limiting conditions below relating to orthorhombic crystals.

(a)

hkl	None	$h00$	$h = 2n$
$0kl$	None	$0k0$	$k = 2n$
$h0l$	None	$00l$	None
$hk0$	None		

(b)

hkl	None	$h00$	None
$0kl$	$k = 2n$	$0k0$	$k = 2n$
$h0l$	None	$00l$	None
$hk0$	None		

(c)

hkl	$h + k + l = 2n$	$h00$	$h = 2n$
$0kl$	$k = 2n, l = 2n$	$0k0$	$k = 2n$
$h0l$	$h + l = 2n$	$00l$	$l = 2n$
$hk0$	$h + k = 2n$		

3.16. (a) Write the independent conditions limiting possible X-ray reflections for the following space groups: (i) $P2_1/a$; (ii) Pc; (iii) $C2$; (iv) $P2_122$; (v) $Pcc2$; (vi) *Imam*. In each case, write the symbols of the space groups, if any, in the same crystal system with the same limiting conditions. (b) Write the conditions limiting possible X-ray reflections in the monoclinic space group $P2_1/n$ (non-standard setting). (c) Give the conventional symbols for the space groups $A2/a$ and $B2_122_1$.

3.17. (a) Space group *Pcab* corresponds to the non-standard setting **acb**, that is, **a** along x, $-$**c** along y, and **b** along z. What is the symbol in the standard (**abc**) setting? (b) What is the essential difference between the space groups represented by the standard symbols *Pmna* and *Pnma*? What are their full symbols?

3.18. The absorption correction for a crystal ground into a sphere of radius r is dependent on r, μ, and θ. Assume that extinction effects are negligible and determine the ideal intensity for an hkl reflection, given that the measured intensity less background is 56.3, and that $r = 0.11$ mm and $\mu = 18.2 \times 10^3$ m^{-1}. For this reflection, $\theta = 30°$, and some tabulated data are listed above, corresponding to the numerical integration $A = \{(1/V) \int dx \int dy \int \exp[-\mu\ (r_0 + r)]\ dz\}^{-1}$, where r_0 and r are, respectively, the incident and diffracted paths lengths in the crystal. Include the θ-dependent Lorentz and polarization corrections.

Transmission factors A for a sphere of radius R and linear absorption coefficient μ

	θ/°		
μR	25	30	35
1	3.88	3.79	3.70
2	10.9	10.0	9.26
3	22.4	19.5	17.1
4	37.2	31.0	26.3

3.19. For space group $P6_3/m$, what are (a) the Schönflies point group symbol, (b) the full Hermann–Mauguin point-group and space-group symbols, (c) the crystal system, (d) the crystal class, (e) the lattice, and (f) the conventional unit cell?

3.20. Using the coordinates of the general equivalent positions for space group $P4nc$, Fig. 2.37, derive (a) the geometrical structure factors, (b) the amplitude symmetry, (c) the phase-angle symmetry.

References

1. See Bibliography, International tables for X-ray crystallography, vol 4
2. Gilfrich JV et al (1995) Advances in X-ray analysis, vol 39. In: Proceedings of the 45th annual conference on applications of X-ray analysis, Colorado Springs
3. http://blog.the-scientist.com/2011/04/11/multipole-wigglers/
4. Karsch S et al (2010) Max-Planck Institüt für Quantenoptik. In: Osterhoff Jens (ed) Laser-plasma acceleration. Universität Hamburg, Hamburg
5. See Bibliography: James (1958), Woolfson (1977) or http://www.gwyndafevans.co.uk/thesis-html/node11.html
6. Ladd M (1998) Introduction to physical chemistry, 3rd edn. Cambridge University Press, Cambridge
7. (1962) International tables for X-ray crystallography, vol IV. Kynoch Press
8. Ewald PP (1913) Z Phys 14:465
9. Holmes KC (2006) Nature 440:149
10. See Bibliography, Chapter 1, Henry et al (1965)

Bibliography: Synchrotron Radiation

Helliwell JR (1992) Macromolecular crystallography with synchrotron radiation. Cambridge University Press, Cambridge

Structure Factor and Intensity

James RW (1958) Optical principles of the diffraction of X-rays: the crystalline state, vol 2. Bell, London

Prince E, Wilson AJC (1999) International tables for X-ray crystallography, vol C, 2nd edn. Kluwer Academic, Dordrecht

Woolfson MM (1977) An introduction to X-ray crystallography, 2nd edn. Cambridge University Press, Cambridge

Atomic Scattering Factors

Ibers JA, Hamilton WC (eds) (1974) International tables for X-ray crystallography, vol 4. Kynoch Press, Birmingham